Molecular Cell

Article

MORG1 limits mTORC1 signaling by inhibiting Rag GTPases

Graphical abstract

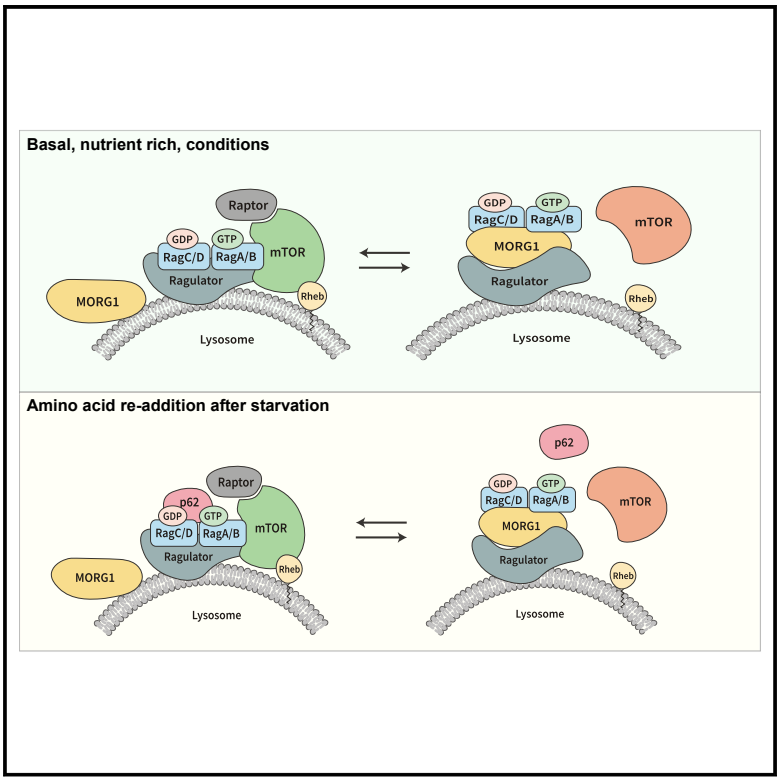

Highlights

- MORG1 binds to active Rag GTPases to inhibit mTORC1 in nutrient-rich conditions
- MORG1-mediated inhibition of mTORC1 allows basal constitutive autophagy
- p62 and MORG1 compete for binding to the Rag GTPases during amino acid restimulation
- Low levels of MORG1 mRNA correlate with reduced survival in several cancers

Authors

Yakubu Princely Abudu, Athanasios Kournoutis, Hanne Britt Brenne, Trond Lamark, Terje Johansen

Correspondence

yakubu.p.abudu@uit.no (Y.P.A.), terje.johansen@uit.no (T.J.)

In brief

Abudu et al. report that the WD-domain repeat protein MORG1 restricts mTORC1 signaling during nutrient-rich conditions, and this facilitates basal autophagy. MORG1 interacts with active Rag GTPases and inhibits the lysosomal recruitment of mTORC1. Moreover, MORG1 and p62/SQSTM1 act antagonistically on mTORC1 activation upon amino acid withdrawal and restimulation.

Abudu et al., 2024, Molecular Cell *84*, 552–569
February 1, 2024
https://doi.org/10.1016/j.molcel.2023.11.023

CellPress

CellPress
OPEN ACCESS

Molecular Cell

Article

MORG1 limits mTORC1 signaling by inhibiting Rag GTPases

Yakubu Princely Abudu,[1,2,*] Athanasios Kournoutis,[1] Hanne Britt Brenne,[1] Trond Lamark,[1] and Terje Johansen[1,3,*]
[1]Autophagy Research Group, Department of Medical Biology, University of Tromsø-The Arctic University of Norway, Tromsø, Norway
[2]Nanoscopy Group, Department of Physics and Technology, University of Tromsø-The Arctic University of Norway, Tromsø, Norway
[3]Lead contact
*Correspondence: yakubu.p.abudu@uit.no (Y.P.A.), terje.johansen@uit.no (T.J.)
https://doi.org/10.1016/j.molcel.2023.11.023

SUMMARY

Autophagy, an important quality control and recycling process vital for cellular homeostasis, is tightly regulated. The mTORC1 signaling pathway regulates autophagy under conditions of nutrient availability and scarcity. However, how mTORC1 activity is fine-tuned during nutrient availability to allow basal autophagy is unclear. Here, we report that the WD-domain repeat protein MORG1 facilitates basal constitutive autophagy by inhibiting mTORC1 signaling through Rag GTPases. Mechanistically, MORG1 interacts with active Rag GTPase complex inhibiting the Rag GTPase-mediated recruitment of mTORC1 to the lysosome. MORG1 depletion in HeLa cells increases mTORC1 activity and decreases autophagy. The autophagy receptor p62/SQSTM1 binds to MORG1, but MORG1 is not an autophagy substrate. However, p62/SQSTM1 binding to MORG1 upon re-addition of amino acids following amino acid's depletion precludes MORG1 from inhibiting the Rag GTPases, allowing mTORC1 activation. MORG1 depletion increases cell proliferation and migration. Low expression of MORG1 correlates with poor survival in several important cancers.

INTRODUCTION

Degradation of cellular components by autophagy is a vital quality control process crucial for cellular homeostasis and prevention of diseases. Autophagy depends on ATG (autophagy-related) proteins conserved from yeast to humans.[1–3] During macroautophagy (hereafter autophagy), double-membrane vesicles, called autophagosomes, form around components to be degraded. Autophagosomes fuse with lysosomes, and the components are degraded and recycled.[4–6] Autophagy occurs constitutively but increases upon cellular stress, such as infection and nutrient starvation. Due to its crucial role, autophagy is strictly controlled, too little or too much can have serious consequences. How autophagy is regulated under various cellular conditions is not entirely clear. An important regulator of autophagy is the mTOR (mechanistic target of rapamycin) complex 1 (mTORC1), the primary regulator of cell growth balancing anabolic and catabolic metabolism.[7,8] mTORC1 controls autophagy initiation and maturation and lysosomal biogenesis.[9–12] mTORC1 is dysregulated in a number of diseases and physiological conditions including cancers, diabetes, obesity, and aging.[7,13–18]

mTORC1 is a multifunctional protein complex comprising serine/threonine protein kinase mTOR, along with several regulatory and structural components including regulatory-associated protein of mTOR (RAPTOR/RPTOR), controlling mTORC1 localization and substrate recruitment.[19–21] mTORC1 further includes mammalian lethal with Sec13 protein 8 (mLST8), important for mTOR stabilization, DEP domain-containing mTOR-interacting protein (DEPTOR), a negative regulator of mTOR, and insulin-responsive inhibitor, PRAS40 (proline-rich AKT substrate of 40 kDa).[19,20,22] mTORC1 activity is regulated by a complex of signal nodes coordinated on the lysosomal surface and activated by growth factors and nutrients. This creates a coincidence detection system. Both growth factors and nutrients must be present to activate mTORC1.[19]

In the presence of nutrients, mTORC1 is recruited to the lysosome through Rag GTPases (Rag A–D), which are themselves anchored to the lysosomal surface by the Ragulator complex (LAMTOR 1–5).[23–28] How nutrient availability drives the anchoring of Rag GTPases to the Ragulator and the concurrent recruitment of mTORC1 is not fully understood. Growth factors activate Rheb GTPase on the lysosomal surface, and Rheb activates the kinase activity of mTOR when mTORC1 is recruited to the lysosome.[19,29,30] Activated mTORC1 regulates cell growth by promoting protein synthesis through phosphorylation of proteins regulating translation including ribosomal S6 kinase 1 (S6K1) and eukaryotic translation initiation factor 4E-binding protein 1 (4E-BP1) while inhibiting protein degradation by phosphorylating ATG proteins involved in autophagy initiation, maturation, and lysosomal biogenesis.[9,10,19,31–36] When nutrients are scarce, mTORC1 is inactivated, allowing autophagosome formation and degradation of cytoplasmic contents to replenish cellular needs. Several studies provide insights into how nutrients such as

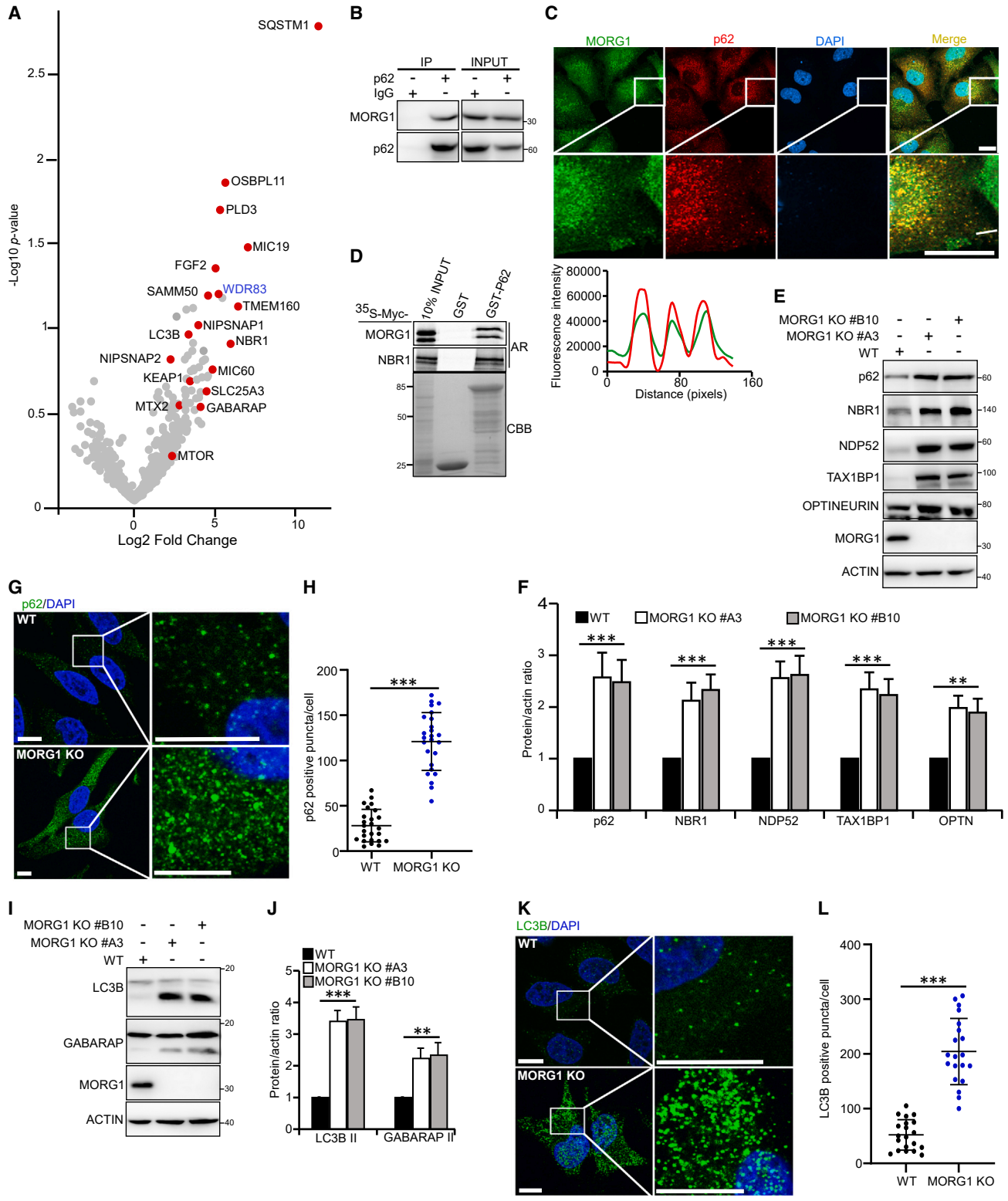

Figure 1. MORG1 interacts with p62/SQSTM1 and depletion of MORG1 inhibits basal autophagy flux

(A) Volcano plot of p62-interacting partners identified and quantified by mass spectrometry from p62 KO HEK293 cells reconstituted with EGFP-tagged p62 and immunoprecipitated with GFP-Trap from four independent experiments (see Table S1).

(B) Co-immunoprecipitation of endogenous p62 and MORG1 from HeLa cells.

(legend continued on next page)

amino acids regulate mTORC1 and autophagy.[7,19,34] How mTORC1 is regulated during nutrient availability to allow constitutive basal autophagy is not understood.

In this study, we identified the WD-repeat protein mitogen-activated protein kinase organizer 1 (MORG1) as an interactor of selective autophagy receptor SQSTM1/p62. We discovered that MORG1 inhibits mTORC1 activity enabling basal autophagy flux. MORG1 interacts directly with Ragulator and active Rag GTPases and controls the spatiotemporal localization of mTORC1 to the lysosomal surface. SQSTM1/p62 interacts with MORG1 and Rag GTPases upon re-addition of amino acids following amino acid deprivation to counteract MORG1-mediated inhibition and allows the activation of mTORC1. Consequently, MORG1 fine-tunes the activity mTORC1 both during amino acid availability and scarcity.

RESULTS

MORG1 interacts with p62/SQSTM1, but it is not an autophagy substrate

To identify new interaction partners and autophagic cargoes of SQSTM1/p62, lysates from HEK293 and mouse embryonic fibroblast (MEF) cells knockout (KO) for p62 reconstituted with EGFP-p62 were immunoprecipitated using GFP-Trap, followed by mass spectrometric identification of precipitated proteins (Figures 1A and S1A; Tables S1 and S2). We identified MORG1 (aka WD-repeat-domain-containing protein 83 [WDR83]), as a candidate interaction partner of p62. MORG1 is reported to bind to MEK-binding partner 1 (MP1), a scaffold protein associated with mitogen-activated protein kinase and extracellular-signal-regulated kinase (MEK) pathways.[37,38] MORG1 also binds to prolyl-hydroxylase 3 (PHD3), a critical component in regulating hypoxic responses, and cell polarity adaptor protein Par6.[39,40] MORG1 co-immunoprecipitated with endogenous SQSTM1/p62 (Figure 1B), and vice versa (Figure S1B). MORG1 and p62 colocalize in HeLa cells (Figure 1C) and bind directly to each other (Figure 1D).

To test whether MORG1 is a p62 substrate in selective autophagy, we treated both wild-type (WT) and p62 KO HeLa and HEK293 cells with bafilomycin A1 (BafA1) for 24 h and subjected cell lysates to immunoblotting (Figures S1C–S1F). BafA1 is an inhibitor of vacuolar H^+ATPase (V-ATPase), and by preventing acidification and subsequent lysosomal degradation of cargoes, it is used to measure autophagy flux. However, MORG1 was not degraded through the lysosome, and p62 KO did not affect MORG1 levels under basal conditions in HeLa (Figures S1C and S1D) or HEK293 cells (Figures S1E and S1F). Iron shortage activates hypoxia-inducible factors (HIFs) and selective autophagy.[41–45] p62 regulates cellular oxygen sensing by interacting with PHD3 and is rapidly degraded by autophagy in hypoxia.[46,47] Since MORG1 interacts with components of both hypoxia- and ERK signaling pathways, we tested whether p62 affected MORG1 levels during the activation of HIF (HIF1A) signaling. Consequently, we treated WT and p62 KO HeLa cells with the iron chelator deferiprone (DFP). KO of p62 had no effect on DFP-induced HIF1A or MORG1 degradation during iron shortage (Figures S1G and S1H).

MORG1 KO inhibits autophagy flux

We generated MORG1 KO using CRISPR-Cas9 in both HEK293 and HeLa cell lines. Interestingly, KO of MORG1 led to the accumulation of p62 and other selective autophagy receptors under basal conditions in both HeLa (Figures 1E and 1F) and HEK293 cells (Figures S1I and S1J). Both diffuse and punctate p62 structures (p62 bodies) accumulated in MORG1 KO cells pointing to disruption in the basal turnover of p62 (Figures 1G and 1H). Human ATG8 (hATG) proteins LC3B and GABARAP increased substantially in MORG1 KO cells (Figures 1I–1L, S1K, and S1L). This accumulation was not exerted at the transcriptional level since qPCR (Figures S1M and S1N) showed no significant changes in mRNA levels of these proteins between MORG1 KO and WT cells. Therefore, MORG1 affects protein levels of p62 and hATG8 proteins under basal conditions.

Lipidated LC3B (LC3B-II) is degraded by autophagy, migrates faster in gels than LC3B-I, and is used to measure autophagic flux in cells. Treatment of WT and MORG1 KO HeLa cells with BafA1 for 24 h resulted in a strong decrease in autophagy flux of both p62 and NDP52 (Nuclear domain 10 protein 52) in MORG1 KO cells compared with WT cells (Figures 2A–2C). We obtained similar results in HEK293 WT and MORG1 KO cells (Figures S2A and S2B). Thus, MORG1 is required for efficient basal lysosomal turnover of these proteins (Figure 2C). We also examined lysosomal turnover during iron shortage and starvation. Lysosomal degradation of p62 and NCOA4 was significantly reduced in MORG1 KO cells treated with DFP for 24 h compared with WT cells (Figures 2D and 2E). However, degradation of p62 and NDP52 was not significantly affected after placing HeLa cells in Hanks' balanced salt solution (HBSS) for 3 h (Figures S2C and S2D). Similarly, HBSS-induced degradation of p62 in HEK293 cells was not affected (Figures S2E and

(C) HeLa cells were stained with antibodies to endogenous p62 and MORG1. Line profile colocalization plot below represents fluorescence intensity against distance. Scale bars, 20 μm.

(D) MORG1 interacts directly with p62/SQSTM1. GST pull-down assay using *in vitro*-translated Myc-tagged proteins labeled with [^{35}S]-methionine and GST-p62 immobilized on glutathione Sepharose beads. Bound proteins were analyzed by autoradiography (AR) and GST proteins visualized by Coomassie brilliant blue (CBB).

(E and F) HeLa wild-type (WT) and two clones of MORG1 KO cells analyzed by immunoblotting of selective autophagy receptors (SLRs) (E) and quantified (F). Values are mean ± SD. ***$p < 0.001$; **$p < 0.005$; (n = 3) ANOVA.

(G and H) HeLa WT and MORG1 KO cells stained with antibody to endogenous p62 analyzed by high resolution confocal microscopy (G), p62 positive puncta were quantified (H). Values are mean ± SD. ***$p < 0.001$; (n = 25) t test.

(I and J) HeLa wild-type (WT) and two clones of MORG1 KO cells analyzed by immunoblotting of human ATG8 proteins (hATG8s) (I) and the lipidated form quantified (J). Values are mean ± SD. ***$p < 0.001$; **$p < 0.005$; (n = 3) ANOVA.

(K and L) HeLa WT and MORG1 KO cells stained for endogenous LC3B (K). LC3B-positive puncta were quantified (L). Values are mean ± SD. ***$p < 0.001$; (n = 25) t test. See also Figure S1.

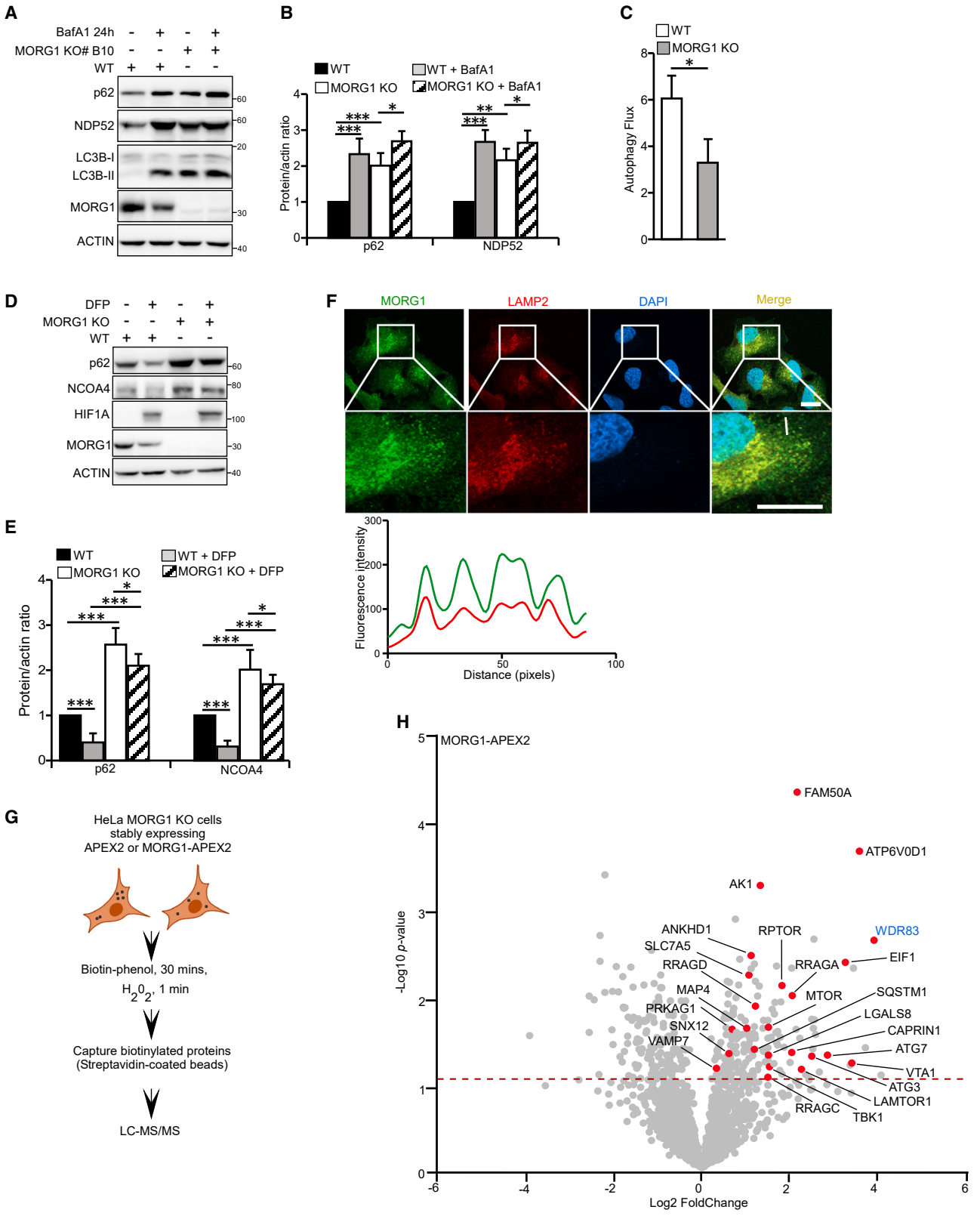

(legend on next page)

S2F). Hence, MORG1 promotes autophagy flux and affects basal- and iron-induced autophagy, but not starvation-induced autophagy.

MORG1 localizes to lysosomal compartments

Confocal microscopy of HeLa cells stained with antibodies to endogenous MORG1 and LAMP2 revealed that MORG1 localized to the cytoplasm with weak nuclear distribution. MORG1 localizes significantly to lysosomal compartments, colocalizing with LAMP2 (Figure 2F). MORG1 KO and WT cells had similar levels of lysosomal membrane proteins LAMP1 and LAMP2 (Figures S2G and S2H). MORG1 KO did not affect lysosomal trafficking or degradation as assessed by the dye quenched-bovine serum albumin (DQ-BSA) trafficking assay[48] (Figures S2I and S2J). Thus, the effect of MORG1 on basal degradation of p62 and other ATG proteins is not exerted through a direct effect on lysosomal trafficking or degradation.

We combined standard immunoprecipitation and APEX2-based proximity labeling with quantitative proteomic analysis to systematically identify potential interacting partners of MORG1. First, we reconstituted MORG1 KO cells with Myc-tagged MORG1 and performed a standard immunoprecipitation using Myc trap and identified interaction partners with mass spectrometry (Figure S2K; Table S3). Second, we performed APEX2 proximity ligation assay (Figure 2G) using MORG1-APEX2 stably expressed in MORG1 KO HeLa cells and identified proximity partners with mass spectrometry (Figure 2H; Table S4). Consistently, we identified components of the mTORC1 signaling pathways as putative interaction partners of MORG1 including mTOR, Raptor, Rag proteins, and LAMTOR1 (Figures 2H and S2K; Tables S3 and S4). Interestingly, one of the earliest known partners of MORG1, MP1, is now known as LAMTOR 3.[37,49,50]

MORG1 inhibits mTORC1

Confocal microscopy of MORG1 KO cells reconstituted with MORG1-EGFP cells showed colocalization between mTOR and MORG1 (Figure 3A). We then analyzed the activity of mTORC1 in WT and MORG1 KO HeLa cells. Phosphorylation of mTOR S2448 monitors the activity of S6K1, a mTORC1 substrate that phosphorylates mTOR S2448 by a feedback loop of unknown function.[51–55] Phosphorylation of mTOR S2448 was increased in MORG1 KO relative to WT cells (Figures 3B and 3C). Also, phosphorylation of two well-characterized mTORC1 substrates, ribosomal S6K1 and eukaryotic translation initiation factor 4E-BP1, was increased (Figures 3D and 3E). mTOR is a key component of both mTORC1 and mTORC2 complexes.[19,20,56,57] mTORC2 phosphorylation of AKT (PKB) on S473 in the hydrophobic motif is required for AKT function.[58,59] There was no significant change in the levels of phosphorylated AKT in MORG1 KO cells compared with WT (Figures S3A and S3B), suggesting that MORG1 specifically affects mTORC1 signaling. mTORC1 regulates autophagy by phosphorylating key autophagy proteins including ULK1 complex components required for autophagy initiation,[9,33] and lysosomal transcription factors EB and E3 (TFEB and TFE3) required for lysosomal biogenesis.[11,60–62] Phosphorylation of ULK1 at S757 was significantly increased in MORG1 KO cells compared with WT (Figures 3D and 3E), as were phosphorylation of TFEB (at S211) and TFE3 (Figures 3D and 3E). Conversely, MORG1 overexpression suppressed mTORC1 activity and promoted autophagy as measured by increased degradation of p62 (Figures 3F and 3G). Degradation of p62 and LC3B induced by overexpression of MORG1 is comparable to starvation-induced degradation of these proteins (Figures S3C and S3D). Overexpression of MORG1 reduced phosphorylation levels of S6K1 and 4E-BP1 (Figures 3H, 3I, S3E, and S3F). Furthermore, treatment of MORG1 KO cells with mTOR inhibitors Rapamycin or Torin1 reduced the elevated protein levels of p62 and NDP52 (Figures S3G and S3H). In conclusion, MORG1's inhibition of mTORC1 enables basal autophagy flux.

mTORC1 activity is regulated by amino acids. Leucine stimulates mTORC1 activity through the Rag GTPases.[24,25,28,63] MORG1 KO induced a dramatic increase in leucine-stimulated mTORC1 activity in HeLa cells (Figure 3J). S6K1- and 4E-BP1 phosphorylation increased in response to a broad range of leucine concentrations. Phosphorylation of these mTORC1 substrates was even detected in the absence of leucine in MORG1 KO HEK293 cells (Figure S3I). Unlike HeLa WT cells, no reduction of mTORC1 activity was seen upon the growth of MORG1 KO cells in a serum-free medium (Figures S3J and S3K). MORG1 KO did not affect ERK signaling (Figure S3J). Hence, MORG1 also modulates amino acid-dependent mTORC1 signaling.

MORG1 restricts cell proliferation and migration in breast cancer

mTORC1 is a primary regulator of cell growth.[7,64–67] Hence, we asked whether MORG1 had any effect on cell growth and proliferation. Indeed, MORG1 KO significantly increased cell proliferation in both HeLa (Figure 4A) and HEK293 cells (Figure S4A).

Figure 2. MORG1 promotes basal autophagy flux and localizes to the lysosome

(A and B) HeLa WT and MORG1 KO cell lines treated with bafilomycin A1 for 24 h analyzed by immunoblotting of indicated proteins (A) and quantified (B). Values are mean ± SD. ***p < 0.001; **p < 0.005; *p < 0.01; (n = 3) ANOVA.

(C) Ratio of (LC3B-II + BafA1/actin)/(LC3B-II/actin) after 24 h BafA1 treatment as shown in (A) corresponding to lipidated LC3B turnover or autophagy flux. Values are mean ± SD. *p < 0.01; (n = 3) ANOVA.

(D and E) HeLa WT and MORG1 KO cell lines treated with DFP analyzed by immunoblotting of indicated proteins (D) and quantified (E). Values are mean ± SD. ***p < 0.001; **p < 0.005; *p < 0.01; (n = 3) ANOVA.

(F) HeLa cells stained with antibodies to endogenous MORG1 and LAMP2 analyzed by confocal microscopy. Line profile colocalization plot below represents fluorescence intensity against line distance. Scale bars, 20 μm.

(G) MORG1-APEX2 proximity ligation assay (see STAR Methods).

(H) Volcano plot of MORG1-APEX2 proximity partners identified and quantified (liquid chromatography-tandem mass spectrometry [LC-MS/MS]) from three independent experiments. x and y axes show the $\log_2$ (fold change) and $-\log_{10}$ (p values); t test (n =3 biological replicates per group). Red dots indicate increased proximity to MORG1. Orange stapled line indicate values below the statistical significance cutoff ($p \geq 0.05$) (see Table S4). See also Figure S2.

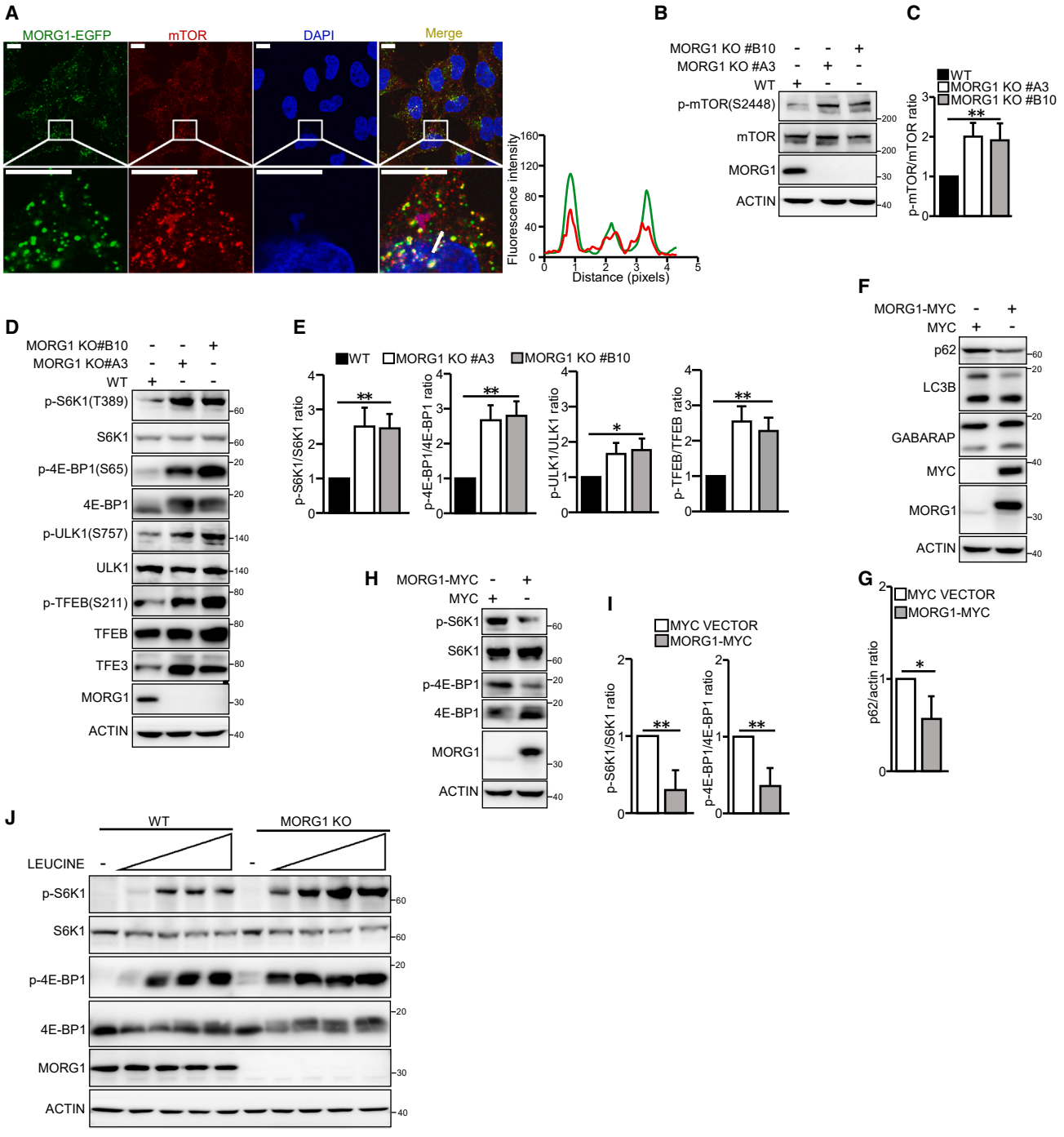

Figure 3. MORG1 inhibits mTORC1 activity

(A) MORG1 KO HeLa cells expressing EGFP-tagged MORG1 immunostained for mTOR. Line profile colocalization plot to the right. Scale bars, 20 μm.

(B and C) HeLa WT and two clones of MORG1 KO cells immunoblotted for mTOR and phosphorylated mTOR (B) and quantified (C). Values are mean ± SD. **p < 0.005; (n = 3) ANOVA.

(D and E) HeLa WT and two clones of MORG1 KO cells immunoblotted for the indicated proteins (D) and quantified (E). Values are mean ± SD. **p < 0.005; *p < 0.01; (n = 3) ANOVA.

(F and G) HeLa cells stably expressing Myc-tagged MORG1 immunoblotted for the indicated proteins (F) and quantified (G). Values are mean ± SD. *p < 0.01; (n = 3) ANOVA.

(legend continued on next page)

Next, we subjected WT and MORG1 KO HeLa and HEK293 cells to an Incucyte-based scratch assay to measure cell migration. When an artificial gap or ''scratch'' is made in a confluent cell monolayer, cells at the edge of this scratch migrate to close the gap.[68,69]

MORG1 KO significantly increased the migration rate of HeLa cells (Figure 4B). This was corroborated by measuring wound closure rate and relative wound density, which were significantly higher for MORG1 KO compared with WT both in HeLa (Figures 4C and 4D) and HEK293 cells (Figures S4B and S4C). Treatment of MORG1 KO cells with Rapamycin or Torin1 significantly reduced the rate of proliferation (Figure 4E) and migration or invasion (Figure 4F). However, inhibition of autophagy, using the ULK1/2 kinase inhibitor MRT68921 or the PIK3C3/Vps34 inhibitor SAR405[70,71] in HeLa WT cells, did not increase cell proliferation rate (Figure S4D) or migration (Figure S4E) compared with untreated MORG1 KO cells. Hence, MORG1 may restrict cell proliferation and migration through a direct effect on mTORC1 signaling.

Aberrant mTORC1 signaling is implicated in several cancers including breast cancers. mTORC1 activity is upregulated in human epidermal growth factor receptor 2 (HER2)-positive breast cancer contributing to cancer progression, proliferation, and metastasis.[15,72–75] Interestingly, depletion of MORG1 increased cell proliferation (Figures 4G and S4F) and migration rates in HER2-positive breast cancer cell lines SKBR3 and BT474 (Figures 4H, 4I, S4G, and S4H). Using the Kaplan-Meier (KM) plotter web resource,[76] we looked at the survival of 180 HER2-positive breast cancer patients and saw a 1.6-fold increased median survival correlating with high levels of MORG1 mRNA (Figure S4I), although there was no statistically significant effect on overall survival. Encouraged by this result, we looked for a correlation between MORG1 mRNA levels and survival in other cancers using the Pancancer KM plotter web resource[77] and found a very significant positive effect of increased MORG1 mRNA expression on the survival of bladder carcinoma (BLC), pancreatic ductal adenocarcinoma (PDAC), and cervical squamous cell carcinoma (CSCC) (Figures 4J–4L). There was also a survival benefit in sarcoma (SC) and uterine corpus endometrial carcinoma (UCEC) (Figures S4J and S4K).

MORG1 interacts directly with Rag GTPases and the Ragulator complex

MORG1 interacts with MP1 (LAMTOR3).[37,49,50] Pull-down assays show direct binding of MORG1 to members of the Ragulator complex (Figure S5A). Proximity interactomics revealed mTORC1 components as potential MORG1 interaction partners (Figures 2H and S2K). RagA co-localized strongly with MORG1 in MORG1 KO HeLa cells reconstituted with MORG1-EGFP (Figure 5A), and MORG1 interacted directly with the Rag GTPases (Figure 5B). Immunoprecipitation of endogenous MORG1 co-precipitated all Rag GTPases (Figure 5C). Conversely, all Rag GTPases immunoprecipitated endogenous MORG1, with RagA and RagD binding the strongest to MORG1 (Figure S5B).

Galectins regulate mTORC1 activity in response to endomembrane damage.[78] Galectin 8 localized in proximity to MORG1 (Figure 2H), and we confirmed direct interactions between MORG1 and Galectins with a strong affinity for Galectin 8 (Figure S5C). In conclusion, MORG1 interacts directly with several components of the mTORC1 signaling pathway including the Ragulator complex and Rag GTPases (Figure S5D).

MORG1 interacts with active Rag GTPases

Rag GTPases integrate multiple signals from upstream components to induce lysosomal recruitment of mTORC1.[24,25] They form obligate heterodimers of RagA/B bound to RagC/D.[79,80] The heterodimer is active and recruits mTORC1 to the lysosome only when RagA/B is bound to guanosine triphosphate (GTP) and RagC/D is bound to guanosine diphosphate (GDP). This unique locking mechanism stabilizes an active conformation of GTP-bound RagA/B linked to GDP-bound RagC/D and an inactive conformation of GDP-bound RagA/B linked to GTP-bound RagC/D.[27,81,82] We asked whether the nucleotide-loading state of monomeric Rag GTPases affected their interaction with MORG1. Thus, we stably expressed WT Rag GTPases, constitutively active and inactive mutants, in HeLa cells and performed Myc-Trap analysis. Interestingly, MORG1 interacted strongly with both WT RagA and constitutively active GTP-bound RagA ($RagA^{GTP}$; RagA Q66L), but not with inactive GDP-bound RagA ($RagA^{GDP}$; RagA T21L) (Figure 5D). In contrast, MORG1 interacted only weakly with WT RagC and inactive $RagC^{GTP}$ (RagC Q120L), but more with active $RagC^{GDP}$ (RagC S75L) (Figure 5D, lane 6). The reverse was observed for RagB and RagD (Figure S5E). MORG1 interacted weakly with WT and inactive $RagB^{GDP}$ (RagB T54L), but more with active $RagB^{GTP}$ (RagB Q99L) (Figure S5E). Similarly, MORG1 interacted strongly with WT and active $RagD^{GDP}$ (RagD S77L) but weakly with inactive $RagD^{GTP}$ (RagD Q121L) (Figure S5E). We then tested whether MORG1's affinity for Rag GTPases is affected by the nucleotide state of the heterodimers. MORG1 bound strongly to the WT RagA-RagC heterodimer, but not to inactive $RagA^{GDP}$-containing heterodimers (Figure 5E). Furthermore, MORG1 bound strongly to the active $RagA^{GTP}$-$RagC^{GDP}$ heterodimer, but not to the inactive $RagA^{GDP}$-$RagC^{GTP}$ heterodimer (Figure 5E). Similarly, MORG1 interacted strongly with the heterodimer containing WT or active $RagB^{GTP}$, but not the heterodimer containing inactive $RagB^{GDP}$ (Figure S5F). MORG1 also binds the heterodimer containing WT or active $RagD^{GDP}$, but not the inactive $RagB^{GDP}$-$RagD^{GTP}$ heterodimer (Figure S5F). Since MORG1 binds active Rag GTPase dimers, we tested the interaction between MORG1 and the Rag GTPases in conditions of amino acid scarcity and availability. Availability of amino acids stimulates the formation of active Rag heterodimers, whereas amino acid removal inactivates Rag dimers.[24,25,28,83,84] In the absence of amino acids, endogenous MORG1 weakly interacts with Rag

(H and I) HeLa cells expressing Myc-tagged MORG1 immunoblotted for mTORC1 substrates (H) and quantified (I). Values are mean ± SD. **$p < 0.005$; ($n = 3$) ANOVA.

(J) HeLa WT and MORG1 KO cells grown in amino-acid-free media 1 h and then in media containing 0, 1.04, 5.2, 10.4, 52, or 104 μg/mL leucine for 10 min were immunoblotted for mTORC1 substrates S6K1 and 4E-BP1. See also Figure S3.

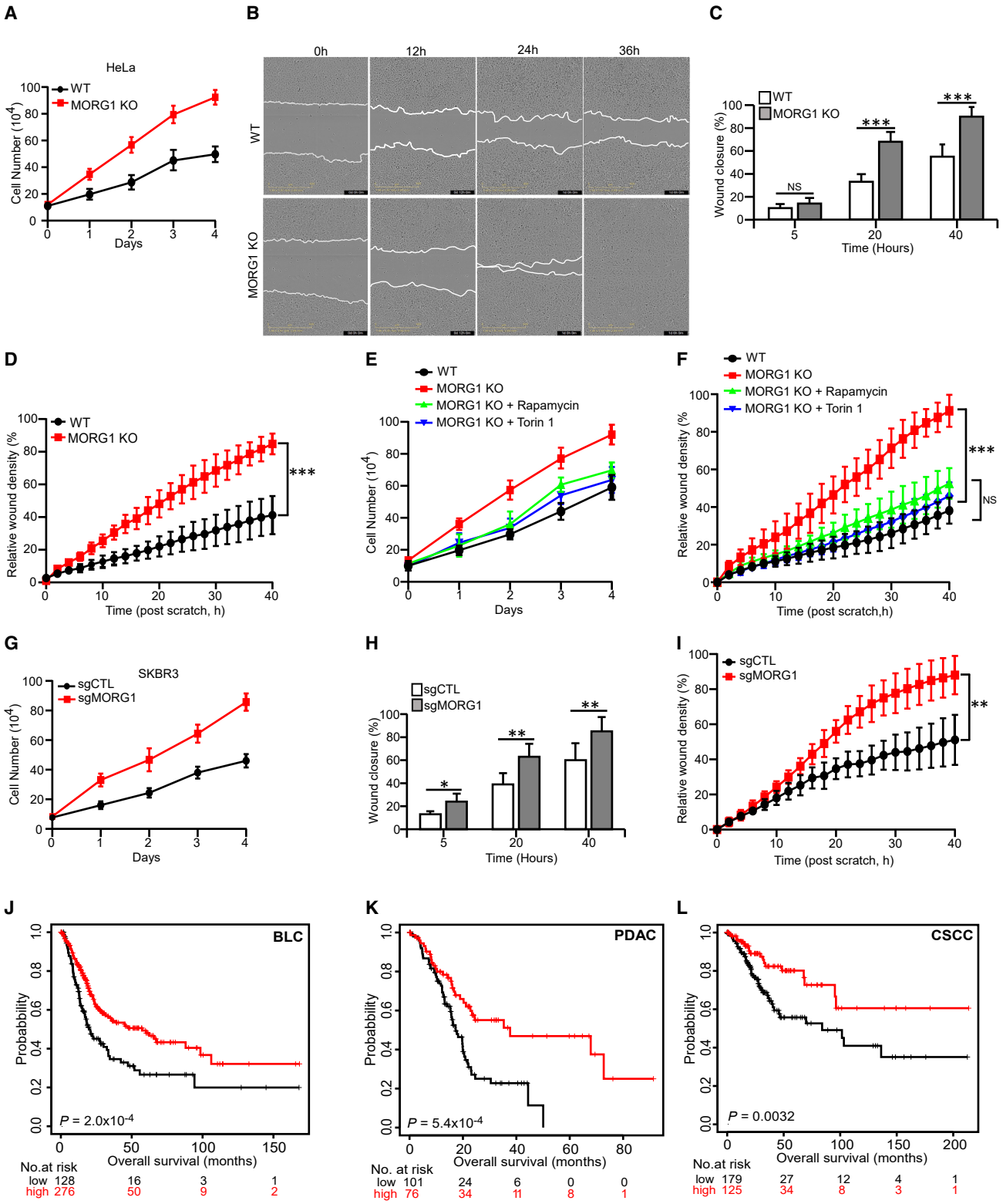

Figure 4. MORG1 negatively regulates cell proliferation and migration

(A) MORG1 KO increases cell proliferation. Equal numbers of HeLa WT and MORG1 KO cells cultured for 4 days. Cell numbers determined by Incucyte cell analysis system.

(legend continued on next page)

GTPases. This interaction increases in the presence of amino acids (Figure 5F). In conclusion, MORG1 interacts preferably with active Rag GTPase complexes. This may modulate how the active Rag GTPases recruit mTORC1 to the lysosome and help fine-tune mTORC1 activity (Figure 5G).

MORG1 inhibits the recruitment of mTORC1 to the lysosome

We hypothesized that MORG1 would affect the recruitment of mTORC1 to lysosomes through interaction with active Rag GTPases. MORG1 KO cells showed an increased localization of mTOR to LAMP2-positive structures (Figures 5H and 5I). This localization was lost upon overexpressing MORG1 in WT HeLa cells (Figures S5G and S5H). Lysosomes analyzed by lysosomal immunoprecipitation (LysoIP)[85] (Figure S6A) had increased levels of mTOR, Raptor, and Rag GTPases in MORG1 KO relative to WT cells, although the cell lysates showed no differences in the levels of these proteins (Figures 6A and 6B). Levels of Ragulator proteins LAMTOR1 and LAMTOR3 were unchanged in the LysoIP and cell lysates (Figures 6A and 6B). Ragulator sits on the lysosome and recruits or anchors Rag GTPases to the lysosome. Subsequently, the Rag GTPases can recruit mTORC1 for activation at the lysosomal surface.[23–28] To explore if MORG1 affects Ragulator-mediated recruitment of Rag GTPases, we stably expressed Myc-tagged LAMTOR1 in WT and MORG1 KO HeLa cells and subjected the cells to Myc-trap. Immunoprecipitation showed increased interaction between Ragulator protein LAMTOR1 and Rag GTPases in MORG1 KO compared with WT cells (Figures 6C and 6D). Higher amounts of RagA, RagC, and Raptor were recovered in immunoprecipitates from MORG1 KO compared with WT cells, whereas the ratio of Ragulator proteins LAMTOR1 and LAMTOR3 was unchanged (Figures 6C and 6D). Similarly, the Myc-trap of cells stably expressing Myc-RagA showed an increased interaction between RagA and LAMTOR1 in MORG1 KO cells compared with WT, whereas the interaction between RagA and RagC did not change (Figures 6E and 6F). However, the interaction between Ragulator components and Rag GTPases decreased in cells overexpressing HA-tagged MORG1 (Figures S6B–S6E). In all cases, the interaction between the components of Ragulator (Figures S6B and S6C) or the Rag GTPases (Figures S6D and S6E) did not change. Hence, MORG1 may modulate the interaction between Ragulator and Rag GTPases. We confirmed this using competitive glutathione S-transferase (GST) pull-down assays. GST-LAMTOR2 immobilized on glutathione Sepharose beads was used in pull-downs with *in-vitro*-translated RagC (Figure S6F) or RagD (Figure S6G), respectively, in the presence of increasing amounts of MORG1. The interaction between RagC and RagD and LAMTOR2 was reduced in the presence of increasing amounts of MORG1. To corroborate these results, we examined the localization of mTOR in HeLa WT and MORG1 KO cells and colocalization between mTOR and MORG1 in the presence and absence of amino acids (Figures 6G, 6H, S6H, and S6I). When cells were starved of amino acids, mTOR was not localized to the lysosome (Figure 6G). However, mTOR localized to the lysosome upon the addition of amino acids in WT cells (Figures 6G and 6H). Interestingly, lysosomal localization of mTOR increased in MORG1 KO cells both in the absence and presence of amino acids compared with WT (Figures 6G and 6H). MORG1 also localized to the lysosome during leucine starvation, whereas mTOR did not (Figures S6H and S6I). Colocalization between mTOR and MORG1 on the lysosome increased with increasing concentrations of leucine (Figures S6H and S6I). In conclusion, MORG1 regulates the spatiotemporal localization of mTORC1 to the lysosomal surface through interactions with both Rag GTPases and Ragulator.

MORG1 inhibits mTORC1 signaling through its N-terminal interaction with Rag GTPases

Reintroduction of MORG1 in MORG1 KO cells reduced phosphorylation levels of mTOR S2448 to WT levels (Figures S6J and S6K). Basal degradation of p62, NDP52, and hATG8 proteins, LC3B and GABARAP, was also restored (Figures S6L–S6O). MORG1 contains seven WD repeats and a short N-terminal arm (Figure S6P). The N-terminal arm is required for binding to Rag GTPases (Figures 6I and S6P). Leucine stimulation demonstrated a stronger increase in mTORC1 activity in MORG1 KO than in WT cells (Figures 3J and S3I). This leucine-stimulated increase in mTORC1 activity was reduced by the reconstitution of MORG1 KO cells with WT MORG1 (Figures 6J and 6K), but not by the mutant lacking the N-terminal amino acids (Figures 6L and 6M). Thus, MORG1 regulates mTORC1 activity during conditions of amino acid availability and scarcity through direct interaction with Rag GTPases.

MORG1 and p62 act antagonistically on mTORC1 activation upon amino acid restimulation

p62/SQSTM1 regulates mTORC1 signaling through interaction with Raptor and Rag GTPases.[86,87] p62 KO does not have any effect on mTORC1 signaling under basal conditions (Figure S7A). In agreement with a previous study by Duran et al.,[86] p62 KO

(B) Incucyte scratch assay of HeLa WT and MORG1 KO cells.
(C and D) Percentage wound closure and relative wound density from Incucyte-based scratch assay in (B). Values are mean ± SD. ***$p < 0.001$; (n = 3) ANOVA.
(E) MORG1 KO HeLa cells treated with 250 nM Rapamycin or 250 nM Torin1 cultured for 4 days and cell numbers were determined.
(F) Relative wound density from Incucyte-based scratch assay of MORG1 KO cells treated with 250 nM Rapamycin or 250 nM Torin1 post scratch. Values are mean ± SD. ***$p < 0.001$; (n = 3) ANOVA.
(G) MORG1 inhibits cell proliferation in HER2-positive breast cancer cells. SKBR3 cells treated with control or MORG1 sgRNA cultured for 4 days and cell numbers determined by Incucyte.
(H and I) Percentage wound closure and relative wound density from the Incucyte-based scratch assay in (G). Values are mean ± SD. **$p < 0.005$; (n = 3) ANOVA.
(J–L) Kaplan-Meier plots showing probabilities of survival of three cancer forms relative to MORG1 mRNA levels. Number of survivals after indicated months are shown. Red or black numbers indicate survivors with high or low MORG1 levels, respectively. BLC, bladder carcinoma; PDAC, pancreatic ductal adenocarcinoma; CSCC, cervical squamous cell carcinoma. See also Figure S4.

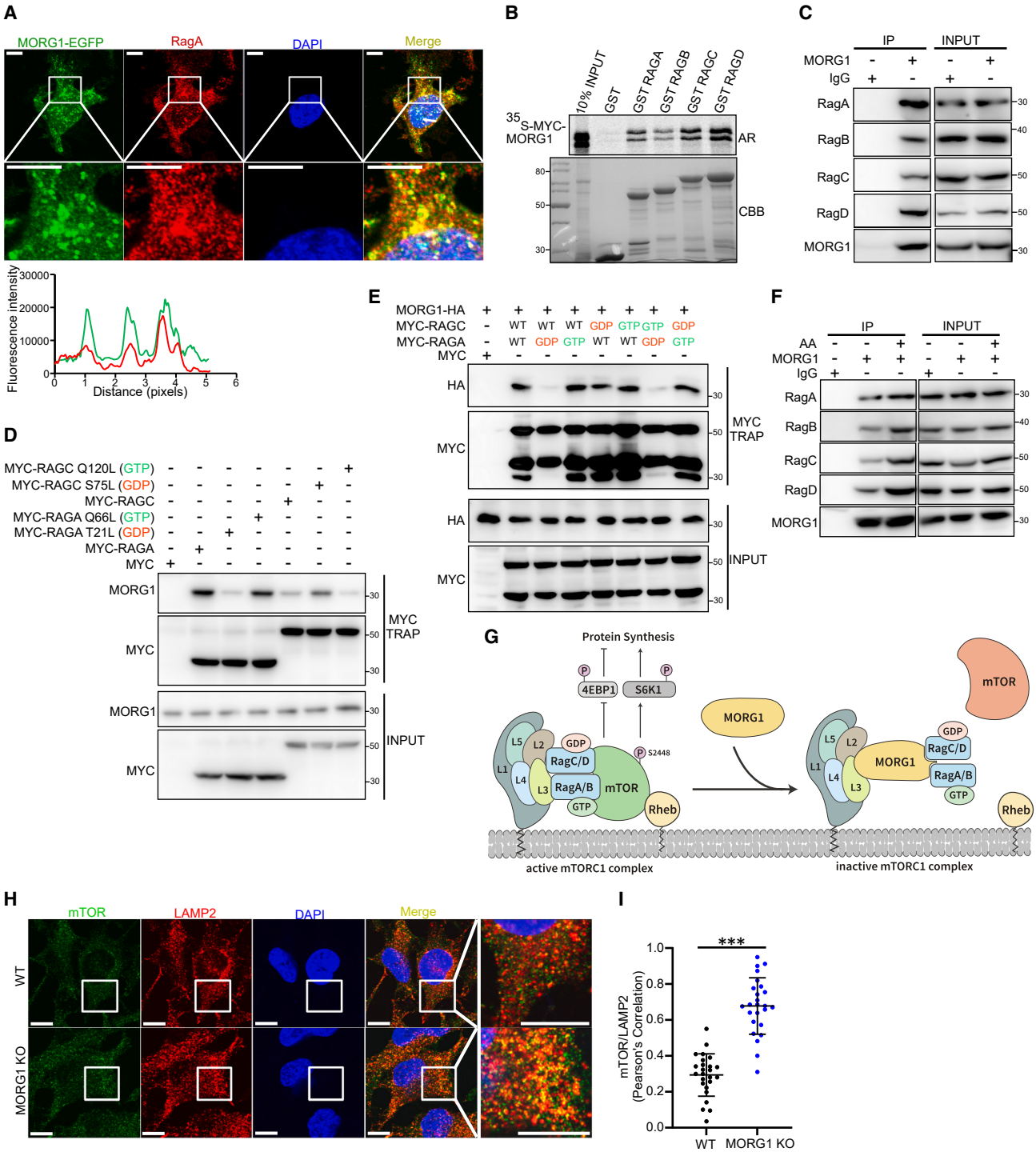

Figure 5. MORG1 interacts with active Rag GTPases and restricts recruitment of mTORC1 to the lysosome

(A) MORG1 KO HeLa cells stably expressing EGFP-tagged MORG1 stained for endogenous RagA. Line profile colocalization plot below. Scale bars, 20 μm.

(B) MORG1 binds directly to Rag GTPases. GST pull-down assay of *in-vitro*-translated Myc-MORG1 with recombinant GST-tagged Rag GTPases. AR, autoradiography; CBB, Coomassie brilliant blue.

(C) Endogenous MORG1 co-immunoprecipitated Rag GTPases from HeLa cell extracts.

(D) MORG1 preferentially interacts with $RagA^{GTP}$ and $RagC^{GDP}$. Myc-tagged WT Rag GTPases and indicated mutants stably expressed in HeLa cells immunoprecipitated using Myc trap with co-immunoprecipitated MORG1 analyzed by immunoblotting.

(E) MORG1 binds to active Rag GTPases. HA-tagged MORG1 co-immunoprecipitated with WT and mutant Rag GTPases expressed in HeLa cells.

(legend continued on next page)

significantly reduced mTORC1 activation following leucine stimulation (Figure 7A). Deletion mapping of p62 identified amino acids 170–256 as the region of p62 binding to MORG1 (Figures S7B and S7C). We confirmed direct interactions between p62 and RagC and RagD (Figure S7D).[86] Surprisingly, the binding of p62 to RagC is via the same region of p62 that binds to MORG1 (Figure S7E). Both WT p62 and the binding-deficient mutant (Δ170–256) were efficiently degraded by autophagy (Figure S7F). However, although p62 KO cells reconstituted with WT p62 restored mTORC1 activity after leucine stimulation, the MORG1- and Rag GTPase-binding-deficient mutant did not (Figure 7B). Since MORG1 and Rag GTPases bind to the same region of p62, we reasoned that MORG1 may restrict p62's role in mTORC1 signaling by competitively inhibiting or modulating p62's interaction with Rag GTPases. Thus, we performed *in vitro* competitive pull-down assays. We immobilized p62 fused with either maltose-binding protein (MBP) on amylose resin (Figure 7C) or with GST on glutathione Sepharose beads (Figure S7G) and performed pull-down assays with *in-vitro*-translated RagD or RagC, respectively, with increasing amounts of MORG1 (Figures 7C and S7G). Binding of Rag GTPases to p62 was dramatically reduced in the presence of increasing amounts of MORG1. Conversely, we immobilized RagC and RagD and tested their interaction with *in-vitro*-translated p62 in the presence of increasing amounts of MORG1 (Figures 7D and S7H). In both cases, p62 binding to Rag GTPases was reduced by MORG1.

We then compared mTORC1 signaling in basal conditions in MORG1 KO-, p62 KO-, or MORG1 + p62 double KO (DKO) cells (Figures 7E and 7F). Although mTORC1 signaling is significantly upregulated in MORG1 KO, there was no change in mTORC1 signaling in p62 KO cells. Interestingly, mTORC1 signaling was also upregulated in MORG1 + p62 DKO cells. By stably expressing Myc-tagged RagC in these KO cells, we discovered that MORG1 KO upregulates the interaction between RagC and Raptor. The interaction was also upregulated in MORG1 + p62 DKO cells (Figures 7G and 7H). Interestingly, p62 KO did not affect the interaction between RagC and Raptor under basal conditions (Figures 7G and 7H), and p62 KO did not affect the interaction between RagC and MORG1 (Figures 7G, S7I, and S7J). Thus, although MORG1 regulates mTORC1 signaling under basal conditions, p62 is dispensable.

We then examined conditions of amino acid withdrawal and re-addition. mTORC1 signaling is significantly higher upon leucine restimulation after amino acid withdrawal compared with basal conditions both in WT and MORG1 KO cells (Figures S7K and S7L). Furthermore, although MORG1 KO upregulated mTORC1 activity upon leucine stimulation, mTORC1 activity was significantly reduced in p62 KO and MORG1+p62 DKO cells (Figures 7I and 7J). Interaction between Myc-RagC and Raptor was very weak in the absence of amino acids, although significantly higher in MORG1 KO cells compared with WT cells (Figures 7K and 7L). Interaction between Myc-RagC and Raptor increased upon restimulation with amino acids in WT and MORG1 KO cells (Figures 7K, 7L, and S7M). No increase was seen in p62 KO cells, and only a partial increase was seen in MORG1 + p62 DKO cells after restimulation with amino acid for 20 min (Figures 7K, 7L, and S7M). Interaction between RagC and MORG1 increased in the absence of p62, whereas interaction between RagC and p62 increased in the absence of MORG1 (Figures 7K, 7L, and S7M). Hence, MORG1 and p62 act antagonistically on mTORC1 activation upon amino acid restimulation.

The interaction between p62 and MORG1 did not change during amino acid withdrawal or restimulation (Figure S7N). Since MORG1 also binds Ragulator, we asked whether p62 could do so. However, p62 does not bind any of the Ragulator proteins (Figure S7O). Mapping the region of MORG1 binding to p62, we found that deleting the N-terminal arm reduced binding, and removal of the three N-terminal WD domains abolished it (Figures S6P and S7P). MORG1 likely interacts with p62 through two surfaces, an N-terminal region, which may explain the competitive interaction with the Rag GTPases, and the region encompassing the WD1–3 domains.

Since MORG1 interacts with p62 under basal conditions (full medium) when p62 is dispensable for mTORC1 signaling, p62 and MORG1 may engage outside the lysosome in interactions likely relevant in other contexts. Hence, we examined colocalization between p62 and MORG1 during basal conditions, amino acid withdrawal, and restimulation (Figures 7M and 7N). In basal conditions, MORG1 co-localized extensively with LAMP2, whereas a few p62 puncta are positive for LAMP2 (Figures 7M and 7N). Several regions with complete overlap between MORG1 and LAMP2 contain only a few p62 dots (Figure 7M, circles in the upper panel). MORG1 and p62 colocalize in several puncta on and outside the lysosome (Figure 7M, arrows in upper panel). Under basal conditions, p62 is dispensable for mTORC1 signaling, whereas MORG1 restricts mTORC1 hyperactivation. However, upon amino acid withdrawal and restimulation, p62 becomes localized extensively to the lysosome (Figures 7M and 7N) and functions in mTORC1 activation. Together, these results suggest a competitive relationship between MORG1 and p62 with respect to interaction with active Rag GTPases and activation of mTORC1 upon amino acid withdrawal and restimulation (Figure 7O).

DISCUSSION

We identified MORG1 as a negative regulator of mTORC1 under nutrient-rich conditions. MORG1 bound to the active Rag GTPases to inhibit mTORC1 localization to the lysosome and phosphorylation of downstream targets. MORG1 interacted both with Ragulator components and Rag GTPases. Although identified as an interactor of autophagy receptor p62/SQSTM1,

(F) Rag GTPases co-immunoprecipitated with endogenous MORG1 from HeLa cells grown in presence or absence of amino acids.
(G) MORG1 inhibits mTORC1 by interacting with active Rag GTPases and Ragulator. In absence of MORG1, mTORC1 signaling becomes hyperactive phosphorylating key substrates.
(H and I) HeLa WT and MORG1 KO cells stained for endogenous mTOR and LAMP2 (H) co-localization quantified using Pearson's correlation coefficients (I). ***$p < 0.001$; ($n = 25$) t test. Scale bars, 10 μm. See also Figure S5.

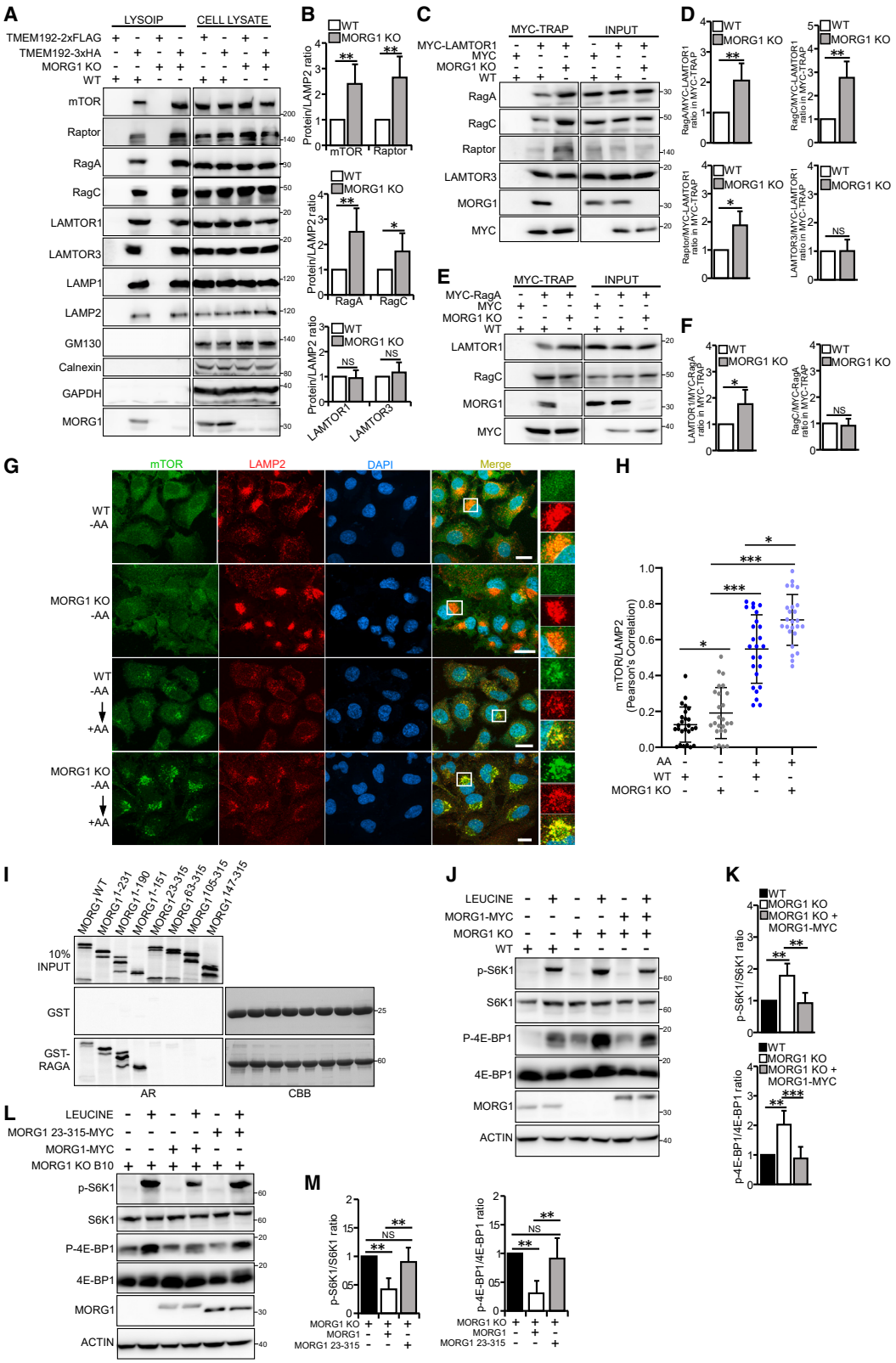

(legend on next page)

MORG1 is not an autophagy substrate. Depletion of MORG1 strongly reduced the basal autophagy flux of p62/SQSTM1, other selective autophagy receptors, and ATG proteins. This occurred without inhibiting starvation-induced autophagy.

The interaction of MORG1 with Rag GTPases and spatiotemporal regulation of mTORC1 add to the complexity of signaling nodes required to fine-tune mTORC1 activity during normal and stress conditions. Amino acid regulation of mTORC1 is well studied.[18,23–28] The presence of amino acids activates the Rag GTPases recruiting mTORC1 to the lysosome. Presence of mTORC1 on the lysosome does not completely block autophagy. Cells still carry our selective autophagy during conditions of amino acid availability signifying the presence of alternative regulation mechanisms for mTORC1. The interaction of MORG1 with both Ragulator and Rag GTPase regulates mTORC1 recruitment to the lysosome in amino acid-replete conditions. MORG1 interacts with active Rag GTPases and restricts how these localize mTORC1 to the lysosome. This spatiotemporal regulation fine-tunes the recruitment of mTORC1 to the lysosome, especially during periods of nutrient availability. This facilitates constitutive basal autophagy during nutrient availability and mTORC1 activation. Rag GTPase dimers are not functionally redundant. Different heterodimers define selective activation of mTORC1 and substrate specificity.[84,88,89] Specifically, the RagA/D dimer specifies mTORC1-dependent phosphorylation of TFEB and stronger association with the lysosome.[84] Our data show that MORG1 KO increased the phosphorylation of TFEB/TFE3 by mTORC1, which inhibits lysosomal biogenesis. MORG1 shows a preference for the Rag A/D dimer (Figures 5B–5F, S5B, S5E, and S5F). This may explain MORG1's ability to fine-tune mTORC1 availability at the lysosome to regulate autophagy. It will be interesting in future studies to determine to what extent other mTORC1-regulated processes may be affected by MORG1.

Other proteins regulate mTORC1 activity through interaction with Rag GTPases or Ragulator. SH3-domain-binding protein 4 (SH3BP4) binds to inactive Rag GTPase to inhibit the formation of the active Rag GTPase complex upon amino acid starvation.[90] p27 interacts with LAMTOR1 and interferes with Ragulator assembly and Rag recruitment, regulating mTORC1 activity during the cell cycle.[8] These may also affect basal autophagy via their effects on mTORC1.

We find MORG1 to regulate the ability of p62/SQSTM1 to activate mTORC1 upon the add-back of amino acids. p62/SQSTM1 is reported as an integral part of the mTORC1-signaling pathway interacting with Raptor and Rag GTPases.[86] p62 is dispensable for mTORC1 signaling in basal conditions but recruited to the lysosome during amino acid withdrawal and restimulation as part of a stress response. Here, we showed that p62/SQSTM1's interaction with the Rag GTPases in human cells is the major driver of mTORC1 activation upon leucine stimulation. MORG1 may regulate the interactions that Rag GTPases have with Ragulator and p62/SQSTM1 (Figure 7O). It is likely that during this response, p62 also supports mTORC1 signaling by other MORG1-independent mechanism(s).

Interestingly, MORG1 may have tumor-suppressive properties for certain cancers. Depletion of MORG1 correlated with increased proliferation and metastatic capabilities in HER2-positive breast cancer cells. Activation of the mTORC1 pathway is common in breast cancer, especially in HER2-positive breast cancer where it contributes to cancer progression, proliferation, and metastasis.[15,72–75] Strikingly, we found a significant correlation between MORG1 mRNA levels and survival for bladder cancer (n = 404), pancreatic ductal carcinoma (n = 177), and cervical squamous carcinoma (n = 304). Hence, the ability of MORG1 to regulate the mTORC1-signaling pathway we have reported here may be important to prevent metastasis and uncontrolled proliferation in several cancers.

Limitations of the study

Further investigation is required to fully understand mechanistically how MORG1 restricts mTORC1 signaling under different conditions (basal versus amino acid restimulation). For example, it will be important to elucidate whether MORG1 affects the nucleotide-loading state of the Rag GTPases. It is also important to determine how MORG1 is tethered to the lysosome. The fact that there is a residual basal autophagy flux in MORG1-depleted cells may point to the presence of MORG1-mTORC1-independent regulation of basal autophagy involving autophagy receptors like p62 and NDP52. This has not been addressed in this study. Moreover, p62 is dispensable for mTORC1 activity under basal conditions, but important under amino acid withdrawal and restimulation, likely as part of a coordinated stress response. In future studies, it will be interesting to elucidate

Figure 6. MORG1 KO increases recruitment of mTOR, Rag GTPases and Raptor to the lysosome

(A and B) LysoIP of HeLa WT and MORG1 KO cells stably expressing TMEM192-3xHA or TMEM192-2xFLAG using anti-HA beads immunoblotted for indicated proteins (A) and quantified (B). Values are mean ± SD. **p < 0.005; *p < 0.01; NS, not significant; (n = 3) ANOVA.

(C and D) Proteins co-immunoprecipitated with Myc-LAMTOR1 from HeLa WT and MORG1 KO cells analyzed by immunoblotting (C) and quantified (D). Values are mean ± SD. **p < 0.005; *p < 0.01; NS, not significant; (n = 3) ANOVA.

(E and F) Proteins co-immunoprecipitated with Myc-RagA from HeLa WT and MORG1 KO cells analyzed by immunoblotting (E) and quantified (F). Values are mean ± SD. **p < 0.005; *p < 0.01; NS, not significant; (n = 3) ANOVA.

(G and H) HeLa WT and MORG1 KO cells grown in amino-acid-free media for 1 h and restimulated with amino acids for 10 min were immunostained for endogenous mTOR and LAMP2 (G) colocalization quantified using Pearson's correlation coefficients (H). ***p < 0.001; **p < 0.005; *p < 0.01; (n = 25) t test. Scale bars, 20 μm.

(I) MORG1 interacts with Rag GTPases through its N-terminal arm. GST pull-down assay of *in-vitro*-translated Myc-MORG1 WT and indicated mutants with recombinant GST-tagged RagA. AR, autoradiography; CBB, Coomassie brilliant blue.

(J and K) Immunoblots (J) with quantifications (K) of mTORC1 substrates from HeLa WT, MORG1 KO and MORG1 KO cells stably reconstituted with MORG1-Myc grown in amino-acid-free media 1 h and then in media containing leucine for 10 min. Values are mean ± SD. ***p < 0.001; **p < 0.005; (n = 3) ANOVA.

(L and M) Immunoblots (L) with quantifications (M) of mTORC1 substrates from MORG1 KO HeLa cells stably reconstituted with MORG1-Myc WT and N-terminal truncated mutant grown as in (J). Values are mean ± SD. **p < 0.005; NS, not significant; (n = 3) ANOVA. See also Figure S6.

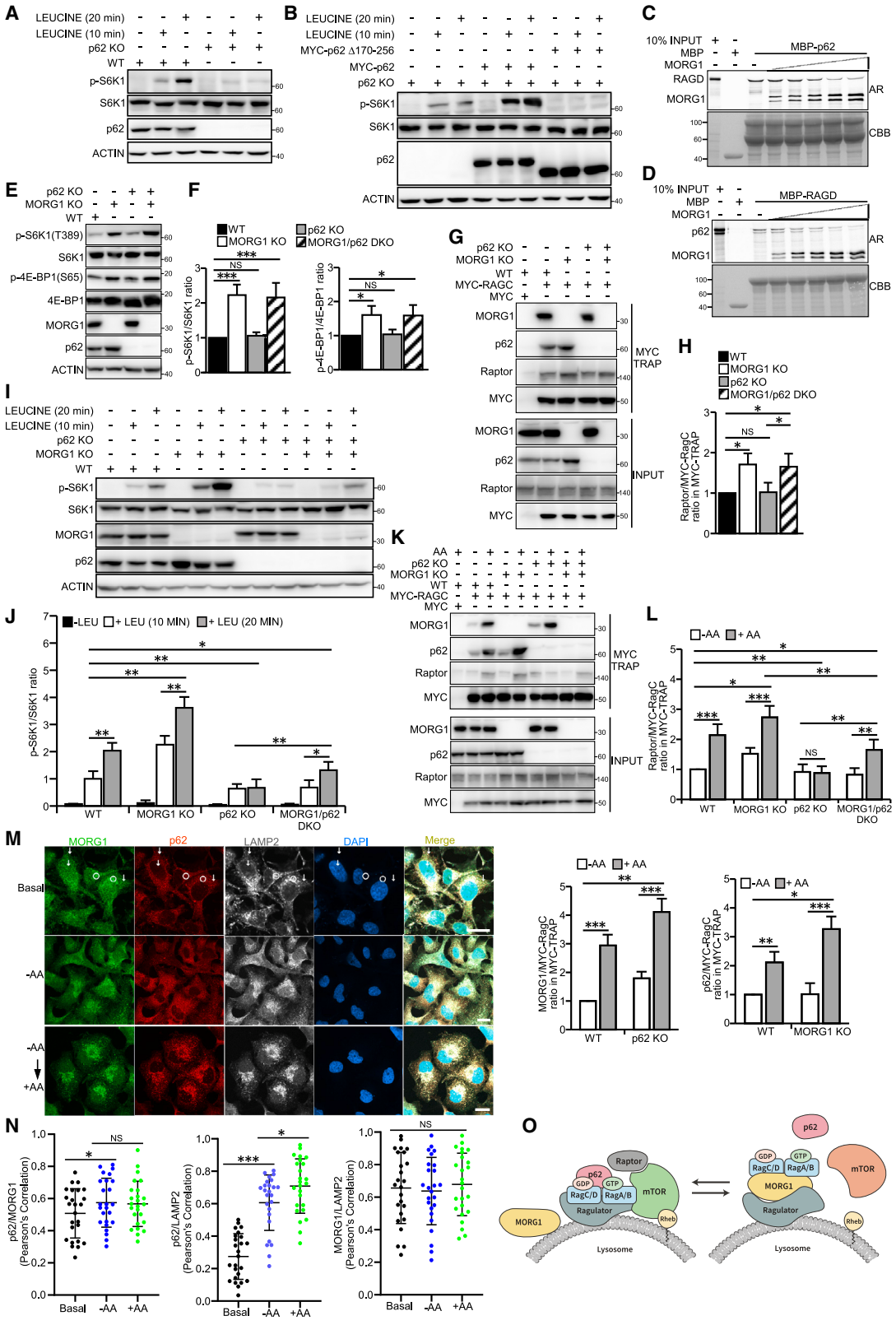

(legend on next page)

how p62 can support mTORC1 signaling via a MORG1-independent mechanism.

STAR★METHODS

Detailed methods are provided in the online version of this paper and include the following:

- KEY RESOURCES TABLE
- RESOURCE AVAILABILITY
  - Lead contact
  - Materials availability
  - Data and code availability
- EXPERIMENTAL MODEL AND STUDY PARTICIPANT DETAILS
  - Cell line models
- METHOD DETAILS
  - Antibodies and reagents
  - Plasmids
  - Cell culture and treatments
  - Generation of human KO cell lines using CRISPR/Cas9 System
  - Generation of stable cell lines and reconstitution of KO cell lines
  - Immunoblotting, immunoprecipitation, and mass spectrometry
  - APEX2 proximity labelling and Streptavidin enrichment for mass spectrometry
  - Confocal microscopy
  - Recombinant protein expression, in vitro translation and GST-pull-down assay
  - Lysosomal immunoprecipitation assay
  - Serum and amino acid stimulation of cells
  - Incucyte-based cell proliferation and migration assay
  - Dye quenched-Bovine serum albumin trafficking assay
  - RT-qPCR analysis
- QUANTIFICATION AND STATISTICAL ANALYSIS

SUPPLEMENTAL INFORMATION

Supplemental information can be found online at https://doi.org/10.1016/j.molcel.2023.11.023.

ACKNOWLEDGMENTS

We thank Jack-Ansgar Bruun and Toril Anne Grønset at the Proteomics and Metabolomics Core Facility (PRiME) for help with mass spectrometric analysis. We thank Kenneth Bowitz Larsen and the Advanced Microscopy Core Facility (AMCF) for help with confocal imaging analysis. Both core facilities are at Institute of Medical Biology, UiT – The Arctic University of Norway. This work was supported by grant number 190214 from the Norwegian Cancer Society and grant number 249884 from The Research Council of Norway to T.J.

AUTHOR CONTRIBUTIONS

Y.P.A. performed most of the experiments, and A.K. and H.B.B. performed some of the experiments. A.K. and T.L. described and prepared the model figures. T.L. and A.K. provided critical discussions and edited the manuscript. Y.P.A. and T.J. designed the research and analyzed data. Y.P.A. and T.J. wrote the final version of the manuscript with help from T.L.

DECLARATION OF INTERESTS

The authors declare no competing interests.

Received: November 18, 2022
Revised: October 2, 2023
Accepted: November 17, 2023
Published: December 15, 2023

REFERENCES

1. Mizushima, N., Yoshimori, T., and Ohsumi, Y. (2011). The role of Atg proteins in autophagosome formation. Annu. Rev. Cell Dev. Biol. *27*, 107–132.

Figure 7. Spatiotemporal regulation of mTORC1 signaling through competitive interactions of MORG1 and p62/SQSTM1 with active Rag GTPases

(A) Immunoblots of mTORC1 substrate S6K1 from HeLa WT and p62 KO cells grown in amino-acid-free media for 4 h and then in leucine-containing media for 10 or 20 min.

(B) Immunoblots of mTORC1 substrate S6K1 from p62 KO cells stably reconstituted with Myc-p62 WT and Δ170–256 mutant grown as in (A).

(C) MORG1 competes with the Rag GTPases for p62 binding. MBP pull-down competition assay with *in-vitro*-translated Myc-RagD and recombinant MBP-p62 in presence of increasing amounts of *in-vitro*-translated Myc-MORG1. AR, autoradiography; CBB, Coomassie brilliant blue.

(D) MORG1 inhibits binding of p62 to the Rag GTPases. MBP pull-down competition assay with *in-vitro*-translated Myc-p62 and MBP-RagD in presence of increasing amounts of *in-vitro*-translated Myc-MORG1.

(E and F) Levels of mTORC1 substrates S6K1 and 4E-BP1 in HeLa WT, MORG1 KO, p62 KO and MORG1/p62 DKO cell lines analyzed by immunoblotting (E) and quantified (F). Values are mean ± SD. ***p < 0.001; *p < 0.01; NS, not significant; (n = 3) ANOVA.

(G and H) Myc-Trap immunoprecipitation from HeLa WT and indicated KO cells stably expressing Myc-RagC analyzed by immunoblotting (G) and Raptor levels quantified (H). Values are mean ± SD. *p < 0.01; NS, not significant; (n = 4) ANOVA.

(I and J) HeLa WT and indicated KO cells grown in amino-acid-free media for 4 h and then in leucine-containing media for 10- or 20 min were analyzed for levels of S6K1 and phosphorylated S6K1 (I) and quantified (J). Values are mean ± SD. **p < 0.005; *p < 0.01; (n = 3) ANOVA.

(K and L) Myc-Trap immunoprecipitation from HeLa WT and indicated KO cells stably expressing Myc-tagged RagC grown in a amino acid-free-media for 4 h and restimulated with amino acids for 20 min. Co-immunoprecipitated proteins were analyzed by immunoblotting (K) and quantified (L). Values are mean ± SD. ***p < 0.001; **p < 0.005; *p < 0.01; NS, not significant; (n = 2) ANOVA.

(M and N) HeLa WT cells grown in full media (basal) or amino acid-free-media for 4 h and restimulated with amino acids for 20 min were stained with antibodies to endogenous MORG1, p62 and LAMP2, and analyzed by confocal microscopy (M) and colocalization between MORG1, p62 and LAMP2 were quantified using Pearson's correlation coefficients (N). ***p < 0.001; *p < 0.01; NS, not significant; (n = 25) t test. Scale bars, 20 μm.

(O) Model of how MORG1 may regulate p62/SQSTM1-Rag GTPase-mTORC1 signaling. Following amino acid withdrawal and restimulation, p62 is recruited to the lysosome to relieve the inhibitory interaction between MORG1 and Rag GTPases, allowing Rag GTPases to effectively recruit mTORC1 to the lysosome for activation. See also Figure S7.

2. Mizushima, N. (2018). A brief history of autophagy from cell biology to physiology and disease. Nat. Cell Biol. *20*, 521–527.
3. Klionsky, D.J., Cregg, J.M., Dunn, W.A., Emr, S.D., Sakai, Y., Sandoval, I.V., Sibirny, A., Subramani, S., Thumm, M., Veenhuis, M., et al. (2003). A unified nomenclature for yeast autophagy-related genes. Dev. Cell *5*, 539–545.
4. Johansen, T., and Lamark, T. (2011). Selective autophagy mediated by autophagic adapter proteins. Autophagy *7*, 279–296.
5. Levine, B., and Kroemer, G. (2019). Biological functions of autophagy genes: a disease perspective. Cell *176*, 11–42.
6. Mizushima, N., Noda, T., Yoshimori, T., Tanaka, Y., Ishii, T., George, M.D., Klionsky, D.J., Ohsumi, M., and Ohsumi, Y. (1998). A protein conjugation system essential for autophagy. Nature *395*, 395–398.
7. Saxton, R.A., and Sabatini, D.M. (2017). mTOR signaling in growth, metabolism, and disease. Cell *168*, 960–976.
8. Nowosad, A., Jeannot, P., Callot, C., Creff, J., Perchey, R.T., Joffre, C., Codogno, P., Manenti, S., and Besson, A. (2020). p27 controls Ragulator and mTOR activity in amino acid-deprived cells to regulate the autophagy–lysosomal pathway and coordinate cell cycle and cell growth. Nat. Cell Biol. *22*, 1076–1090.
9. Kim, J., Kundu, M., Viollet, B., and Guan, K.L. (2011). AMPK and mTOR regulate autophagy through direct phosphorylation of Ulk1. Nat. Cell Biol. *13*, 132–141.
10. Kim, Y.M., Jung, C.H., Seo, M., Kim, E.K., Park, J.M., Bae, S.S., and Kim, D.H. (2015). MTORC1 phosphorylates UVRAG to negatively regulate autophagosome and endosome maturation. Mol. Cell *57*, 207–218.
11. Martina, J.A., Chen, Y., Gucek, M., and Puertollano, R. (2012). MTORC1 functions as a transcriptional regulator of autophagy by preventing nuclear transport of TFEB. Autophagy *8*, 903–914.
12. Settembre, C., Di Malta, C., Polito, V.A., Garcia Arencibia, M.G., Vetrini, F., Erdin, S., Erdin, S.U., Huynh, T., Medina, D., Colella, P., et al. (2011). TFEB links autophagy to lysosomal biogenesis. Science *332*, 1429–1433.
13. Pópulo, H., Lopes, J.M., and Soares, P. (2012). The mTOR signalling pathway in human cancer. Int. J. Mol. Sci. *13*, 1886–1918.
14. Goberdhan, D.C.I., and Boyd, C.A. (2009). mTOR: dissecting regulation and mechanism of action to understand human disease. Biochem. Soc. Trans. *37*, 213–216.
15. Harrison, D.E., Strong, R., Sharp, Z.D., Nelson, J.F., Astle, C.M., Flurkey, K., Nadon, N.L., Wilkinson, J.E., Frenkel, K., Carter, C.S., et al. (2009). Rapamycin fed late in life extends lifespan in genetically heterogeneous mice. Nature *460*, 392–395.
16. Chrienova, Z., Nepovimova, E., and Kuca, K. (2021). The role of mTOR in age-related diseases. J. Enzyme Inhib. Med. Chem. *36*, 1679–1693.
17. Selman, C., Tullet, J.M.A., Wieser, D., Irvine, E., Lingard, S.J., Choudhury, A.I., Claret, M., Al-Qassab, H., Carmignac, D., Ramadani, F., et al. (2009). Ribosomal protein S6 kinase 1 signaling regulates mammalian life span. Science *326*, 140–144.
18. Gu, X., Orozco, J.M., Saxton, R.A., Condon, K.J., Liu, G.Y., Krawczyk, P.A., Scaria, S.M., Harper, J.W., Gygi, S.P., and Sabatini, D.M. (2017). SAMTOR is an S-adenosylmethionine sensor for the mTORC1 pathway. Science *358*, 813–818.
19. Condon, K.J., and Sabatini, D.M. (2019). Nutrient regulation of mTORC1 at a glance. J. Cell Sci. *132*.
20. Aylett, C.H.S., Sauer, E., Imseng, S., Boehringer, D., Hall, M.N., Ban, N., and Maier, T. (2016). Architecture of human mTOR complex 1. Science *351*, 48–52.
21. Hara, K., Maruki, Y., Long, X., Yoshino, K., Oshiro, N., Hidayat, S., Tokunaga, C., Avruch, J., and Yonezawa, K. (2002). Raptor, a binding partner of target of rapamycin (TOR), mediates TOR action. Cell *110*, 177–189.
22. Peterson, T.R., Laplante, M., Thoreen, C.C., Sancak, Y., Kang, S.A., Kuehl, W.M., Gray, N.S., and Sabatini, D.M. (2009). DEPTOR is an mTOR inhibitor frequently overexpressed in multiple myeloma cells and required for their survival. Cell *137*, 873–886.
23. Efeyan, A., Zoncu, R., Chang, S., Gumper, I., Snitkin, H., Wolfson, R.L., Kirak, O., Sabatini, D.D., and Sabatini, D.M. (2012). Regulation of mTORC1 by the Rag GTPases is necessary for neonatal autophagy and survival. Nature *493*, 679–683.
24. Sancak, Y., Peterson, T.R., Shaul, Y.D., Lindquist, R.A., Thoreen, C.C., Bar-Peled, L., and Sabatini, D.M. (2008). The Rag GTPases bind raptor and mediate amino acid signaling to mTORC1. Science *320*, 1496–1501.
25. Sancak, Y., Bar-Peled, L., Zoncu, R., Markhard, A.L., Nada, S., and Sabatini, D.M. (2010). Ragulator-Rag complex targets mTORC1 to the lysosomal surface and is necessary for its activation by amino acids. Cell *141*, 290–303.
26. Bar-Peled, L., Schweitzer, L.D., Zoncu, R., and Sabatini, D.M. (2012). Ragulator is a GEF for the Rag GTPases that signal amino acid levels to mTORC1. Cell *150*, 1196–1208.
27. Shen, K., and Sabatini, D.M. (2018). Ragulator and SLC38A9 activate the Rag GTPases through noncanonical GEF mechanisms. Proc. Natl. Acad. Sci. USA *115*, 9545–9550.
28. Kim, E., Goraksha-Hicks, P., Li, L., Neufeld, T.P., and Guan, K.L. (2008). Regulation of TORC1 by Rag GTPases in nutrient response. Nat. Cell Biol. *10*, 935–945.
29. Inoki, K., Li, Y., Xu, T., and Guan, K.L. (2003). Rheb GTPase is a direct target of TSC2 GAP activity and regulates mTOR signaling. Genes Dev. *17*, 1829–1834.
30. Long, X., Lin, Y., Ortiz-Vega, S., Yonezawa, K., and Avruch, J. (2005). Rheb binds and regulates the mTOR kinase. Curr. Biol. *15*, 702–713.
31. Holz, M.K., Ballif, B.A., Gygi, S.P., and Blenis, J. (2005). mTOR and S6K1 mediate assembly of the translation preinitiation complex through dynamic protein interchange and ordered phosphorylation events. Cell *123*, 569–580.
32. Magnuson, B., Ekim, B., and Fingar, D.C. (2012). Regulation and function of ribosomal protein S6 kinase (S6K) within mTOR signalling networks. Biochem. J. *441*, 1–21.
33. Hosokawa, N., Hara, T., Kaizuka, T., Kishi, C., Takamura, A., Miura, Y., Iemura, S.I., Natsume, T., Takehana, K., Yamada, N., et al. (2009). Nutrient-dependent mTORC1 association with the ULK1-Atg13-FIP200 complex required for autophagy. Mol. Biol. Cell *20*, 1981–1991.
34. Jung, C.H., Ro, S.H., Cao, J., Otto, N.M., and Kim, D.H. (2010). MTOR regulation of autophagy. FEBS Lett. *584*, 1287–1295.
35. Wang, Y., and Zhang, H. (2019). Regulation of autophagy by mTOR signaling pathway. Adv. Exp. Med. Biol. *1206*, 67–83.
36. Schmeisser, K., and Parker, J.A. (2019). Pleiotropic effects of mTOR and autophagy during development and aging. Front. Cell Dev. Biol. *7*, 192.
37. Vomastek, T., Schaeffer, H.J., Tarcsafalvi, A., Smolkin, M.E., Bissonette, E.A., and Weber, M.J. (2004). Modular construction of a signaling scaffold: MORG1 interacts with components of the ERK cascade and links ERK signaling to specific agonists. Proc. Natl. Acad. Sci. USA *101*, 6981–6986.
38. Loeffler, I., and Wolf, G. (2015). The role of hypoxia and Morg1 in renal injury. Eur. J. Clin. Invest. *45*, 294–302.
39. Hopfer, U., Hopfer, H., Jablonski, K., Stahl, R.A.K., and Wolf, G. (2006). The novel WD-repeat protein Morg1 acts as a molecular scaffold for hypoxia-inducible factor prolyl hydroxylase 3 (PHD3). J. Biol. Chem. *281*, 8645–8655.
40. Hayase, J., Kamakura, S., Iwakiri, Y., Yamaguchi, Y., Izaki, T., Ito, T., and Sumimoto, H. (2013). The WD40 protein Morg1 facilitates Par6-aPKC binding to Crb3 for apical identity in epithelial cells. J. Cell Biol. *200*, 635–650.
41. Shah, Y.M., and Xie, L. (2014). Hypoxia-inducible factors link iron homeostasis and erythropoiesis. Gastroenterology *146*, 630–642.
42. Xu, M.M., Wang, J., and Xie, J.X. (2017). Regulation of iron metabolism by hypoxia-inducible factors. Sheng Li Xue Bao *69*, 598–610.

43. Allen, G.F.G., Toth, R., James, J., and Ganley, I.G. (2013). Loss of iron triggers PINK1/Parkin-independent mitophagy. EMBO Rep. *14*, 1127–1135.

44. Mancias, J.D., Wang, X., Gygi, S.P., Harper, J.W., and Kimmelman, A.C. (2014). Quantitative proteomics identifies NCOA4 as the cargo receptor mediating ferritinophagy. Nature *509*, 105–109.

45. Dowdle, W.E., Nyfeler, B., Nagel, J., Elling, R.A., Liu, S., Triantafellow, E., Menon, S., Wang, Z., Honda, A., Pardee, G., et al. (2014). Selective VPS34 inhibitor blocks autophagy and uncovers a role for NCOA4 in ferritin degradation and iron homeostasis in vivo. Nat. Cell Biol. *16*, 1069–1079.

46. Rantanen, K., Pursiheimo, J.P., Högel, H., Miikkulainen, P., Sundström, J., and Jaakkola, P.M. (2013). p62/SQSTM1 regulates cellular oxygen sensing by attenuating PHD3 activity through aggregate sequestration and enhanced degradation. J. Cell Sci. *126*, 1144–1154.

47. Pursiheimo, J.P., Rantanen, K., Heikkinen, P.T., Johansen, T., and Jaakkola, P.M. (2009). Hypoxia-activated autophagy accelerates degradation of SQSTM1/p62. Oncogene *28*, 334–344.

48. Marwaha, R., and Sharma, M. (2017). DQ-Red BSA trafficking assay in cultured cells to assess cargo delivery to lysosomes. Bio Protoc. *7*, e2571.

49. Schaeffer, H.J., Catling, A.D., Eblen, S.T., Collier, L.S., Krauss, A., and Weber, M.J. (1998). MP1: a MEK binding partner that enhances enzymatic activation of the MAP kinase cascade. Science *281*, 1668–1671.

50. Teis, D., Wunderlich, W., and Huber, L.A. (2002). Localization of the MP1-MAPK scaffold complex to endosomes is mediated by p14 and required for signal transduction. Dev. Cell *3*, 803–814.

51. Navé, B.T., Ouwens, M., Withers, D.J., Alessi, D.R., and Shepherd, P.R. (1999). Mammalian target of rapamycin is a direct target for protein kinase B: identification of a convergence point for opposing effects of insulin and amino-acid deficiency on protein translation. Biochem. J. *344*, 427–431.

52. Reynolds, T.H., Bodine, S.C., and Lawrence, J.C. (2002). Control of Ser2448 phosphorylation in the mammalian target of rapamycin by insulin and skeletal muscle load. J. Biol. Chem. *277*, 17657–17662.

53. Scott, P.H., Brunn, G.J., Kohn, A.D., Roth, R.A., and Lawrence, J.C. (1998). Evidence of insulin-stimulated phosphorylation and activation of the mammalian target of rapamycin mediated by a protein kinase B signaling pathway. Proc. Natl. Acad. Sci. USA *95*, 7772–7777.

54. Chiang, G.G., and Abraham, R.T. (2005). Phosphorylation of mammalian target of rapamycin (mTOR) at Ser-2448 is mediated by p70S6 kinase. J. Biol. Chem. *280*, 25485–25490.

55. Holz, M.K., and Blenis, J. (2005). Identification of S6 kinase 1 as a novel mammalian target of rapamycin (mTOR)-phosphorylating kinase. J. Biol. Chem. *280*, 26089–26093.

56. Takahara, T., Amemiya, Y., Sugiyama, R., Maki, M., and Shibata, H. (2020). Amino acid-dependent control of mTORC1 signaling: a variety of regulatory modes. J. Biomed. Sci. *27*, 87.

57. Oh, W.J., and Jacinto, E. (2011). mTOR complex 2 signaling and functions. Cell Cycle *10*, 2305–2316.

58. Sarbassov, D.D., Guertin, D.A., Ali, S.M., and Sabatini, D.M. (2005). Phosphorylation and regulation of Akt/PKB by the rictor-mTOR complex. Science *307*, 1098–1101.

59. Frias, M.A., Thoreen, C.C., Jaffe, J.D., Schroder, W., Sculley, T., Carr, S.A., and Sabatini, D.M. (2006). mSin1 is necessary for Akt/PKB phosphorylation, and its isoforms define three distinct mTORC2s. Curr. Biol. *16*, 1865–1870.

60. Peña-Llopis, S., Vega-Rubin-de-Celis, S., Schwartz, J.C., Wolff, N.C., Tran, T.A.T., Zou, L., Xie, X.J., Corey, D.R., and Brugarolas, J. (2011). Regulation of TFEB and V-ATPases by mTORC1. EMBO J. *30*, 3242–3258.

61. Settembre, C., Zoncu, R., Medina, D.L., Vetrini, F., Erdin, S., Erdin, S., Huynh, T., Ferron, M., Karsenty, G., Vellard, M.C., et al. (2012). A lysosome-to-nucleus signalling mechanism senses and regulates the lysosome via mTOR and TFEB. EMBO J. *31*, 1095–1108.

62. Rabanal-Ruiz, Y., and Korolchuk, V.I. (2018). mTORC1 and nutrient homeostasis: the central role of the lysosome. Int. J. Mol. Sci. *19*.

63. Chen, J., Ou, Y., Luo, R., Wang, J., Wang, D., Guan, J., Li, Y., Xia, P., Chen, P.R., and Liu, Y. (2021). SAR1B senses leucine levels to regulate mTORC1 signalling. Nature *596*, 281–284.

64. Tee, A.R. (2018). The target of rapamycin and mechanisms of cell growth. Int. J. Mol. Sci. *19*, 880.

65. Jewell, J.L., and Guan, K.L. (2013). Nutrient signaling to mTOR and cell growth. Trends Biochem. Sci. *38*, 233–242.

66. Kim, J., and Guan, K.L. (2019). mTOR as a central hub of nutrient signalling and cell growth. Nat. Cell Biol. *21*, 63–71.

67. Laplante, M., and Sabatini, D.M. (2012). MTOR signaling in growth control and disease. Cell *149*, 274–293.

68. Liang, C.C., Park, A.Y., and Guan, J.L. (2007). In vitro scratch assay: a convenient and inexpensive method for analysis of cell migration in vitro. Nat. Protoc. *2*, 329–333.

69. Todaro, G.J., Lazar, G.K., and Green, H. (1965). The initiation of cell division in a contact-inhibited mammalian cell line. J. Cell. Physiol. *66*, 325–333.

70. Petherick, K.J., Conway, O.J.L., Mpamhanga, C., Osborne, S.A., Kamal, A., Saxty, B., and Ganley, I.G. (2015). Pharmacological inhibition of ULK1 kinase blocks mammalian target of rapamycin (mTOR)-dependent autophagy. J. Biol. Chem. *290*, 11376–11383.

71. Pasquier, B. (2015). SAR405, a PIK3C3/VPS34 inhibitor that prevents autophagy and synergizes with MTOR inhibition in tumor cells. Autophagy *11*, 725–726.

72. Lee, J.J.X., Loh, K., and Yap, Y.S. (2015). PI3K/Akt/mTOR inhibitors in breast cancer. Cancer Biol. Med. *12*, 342–354.

73. Miricescu, D., Totan, A., Stanescu-Spinu, I.I., Badoiu, S.C., Stefani, C., and Greabu, M. (2020). PI3K/AKT/mTOR signaling pathway in breast cancer: from molecular landscape to clinical aspects. Int. J. Mol. Sci. *22*, 1–24.

74. Hare, S.H., and Harvey, A.J. (2017). mTOR function and therapeutic targeting in breast cancer. Am. J. Cancer Res. *7*, 383–404.

75. Holloway, R.W., and Marignani, P.A. (2021). Targeting mTOR and glycolysis in HER2-positive breast cancer. Cancers (Basel) *13*.

76. Győrffy, B. (2021). Survival analysis across the entire transcriptome identifies biomarkers with the highest prognostic power in breast cancer. Comput. Struct. Biotechnol. J. *19*, 4101–4109.

77. Nagy, Á., Munkácsy, G., and Győrffy, B. (2021). Pancancer survival analysis of cancer hallmark genes. Sci. Rep. *11*, 6047.

78. Jia, J., Abudu, Y.P., Claude-Taupin, A., Gu, Y., Kumar, S., Choi, S.W., Peters, R., Mudd, M.H., Allers, L., Salemi, M., et al. (2018). Galectins control mTOR in response to endomembrane damage. Mol. Cell *70*, 120–135.e8.

79. Sekiguchi, T., Hirose, E., Nakashima, N., Ii, M., and Nishimoto, T. (2001). Novel G proteins, Rag C and Rag D, interact with GTP-binding proteins, Rag A and Rag B. J. Biol. Chem. *276*, 7246–7257.

80. Schürmann, A., Brauers, A., Massmann, S., Becker, W., and Joost, H.G. (1995). Cloning of a novel family of mammalian GTP-binding proteins (RagA, RagBs, RagB1) with remote similarity to the Ras-related GTPases. J. Biol. Chem. *270*, 28982–28988.

81. Anandapadamanaban, M., Masson, G.R., Perisic, O., Berndt, A., Kaufman, J., Johnson, C.M., Santhanam, B., Rogala, K.B., Sabatini, D.M., and Williams, R.L. (2019). Architecture of human Rag GTPase heterodimers and their complex with mTORC1. Science *366*, 203–210.

82. Shen, K., Choe, A., and Sabatini, D.M. (2017). Intersubunit crosstalk in the Rag GTPase heterodimer enables mTORC1 to respond rapidly to amino acid availability. Mol. Cell *68*, 552–565.e8.

83. Lama-Sherpa, T.D., Jeong, M.H., and Jewell, J.L. (2023). Regulation of mTORC1 by the Rag GTPases. Biochem. Soc. Trans. *51*, 655–664.

84. Gollwitzer, P., Grützmacher, N., Wilhelm, S., Kümmel, D., and Demetriades, C. (2022). A Rag GTPase dimer code defines the regulation of mTORC1 by amino acids. Nat. Cell Biol. *24*, 1394–1406.

85. Abu-Remaileh, M., Wyant, G.A., Kim, C., Laqtom, N.N., Abbasi, M., Chan, S.H., Freinkman, E., and Sabatini, D.M. (2017). Lysosomal metabolomics reveals V-ATPase- and mTOR-dependent regulation of amino acid efflux from lysosomes. Science *358*, 807–813.

86. Duran, A., Amanchy, R., Linares, J.F., Joshi, J., Abu-Baker, S., Porollo, A., Hansen, M., Moscat, J., and Diaz-Meco, M.T. (2011). p62 is a key regulator of nutrient sensing in the mTORC1 pathway. Mol. Cell *44*, 134–146.

87. Linares, J.F., Duran, A., Yajima, T., Pasparakis, M., Moscat, J., and Diaz-Meco, M.T. (2013). K63 polyubiquitination and activation of mTOR by the p62-TRAF6 complex in nutrient-activated cells. Mol. Cell *51*, 283–296.

88. Alesi, N., and Henske, E.P. (2022). Keeping up with the Rag GTPases. Nat. Cell Biol. *24*, 1330–1331.

89. Figlia, G., Müller, S., Hagenston, A.M., Kleber, S., Roiuk, M., Quast, J.P., ten Bosch, N., Carvajal Ibañez, D., Mauceri, D., Martin-Villalba, A., et al. (2022). Brain-enriched RagB isoforms regulate the dynamics of mTORC1 activity through GATOR1 inhibition. Nat. Cell Biol. *24*, 1407–1421.

90. Kim, Y.M., Stone, M., Hwang, T.H., Kim, Y.G., Dunlevy, J.R., Griffin, T.J., and Kim, D.H. (2012). SH3BP4 is a negative regulator of amino acid-rag GTPase-mTORC1 signaling. Mol. Cell *46*, 833–846.

91. Lamark, T., Perander, M., Outzen, H., Kristiansen, K., Øvervatn, A., Michaelsen, E., Bjørkøy, G., and Johansen, T. (2003). Interaction codes within the family of mammalian Phox and Bem1p domain-containing proteins. J. Biol. Chem. *278*, 34568–34581.

92. Jain, A., Lamark, T., Sjøttem, E., Larsen, K.B., Awuh, J.A., Øvervatn, A., McMahon, M., Hayes, J.D., and Johansen, T. (2010). p62/SQSTM1 is a target gene for transcription factor NRF2 and creates a positive feedback loop by inducing antioxidant response element-driven gene transcription. J. Biol. Chem. *285*, 22576–22591.

93. Abudu, Y.P., Shrestha, B.K., Zhang, W., Palara, A., Brenne, H.B., Larsen, K.B., Wolfson, D.L., Dumitriu, G., Øie, C.I., Ahluwalia, B.S., et al. (2021). Samm50 acts with p62 in piecemeal basal- and oxphos-induced mitophagy of sam and micos components. J. Cell Biol. *220*, e202009092.

94. Clausen, T.H., Lamark, T., Isakson, P., Finley, K., Larsen, K.B., Brech, A., Øvervatn, A., Stenmark, H., Bjørkøy, G., Simonsen, A., et al. (2010). p62/SQSTM1 and ALFY interact to facilitate the formation of p62 bodies/ALIS and their degradation by autophagy. Autophagy *6*, 330–344.

95. Sneeggen, M., Pedersen, N.M., Campsteijn, C., Haugsten, E.M., Stenmark, H., and Schink, K.O. (2019). WDFY2 restrains matrix metalloproteinase secretion and cell invasion by controlling VAMP3-dependent recycling. Nat. Commun. *10*, 2850.

96. Princely Abudu, Y.P., Pankiv, S., Mathai, B.J., Håkon Lystad, A., Bindesbøll, C., Brenne, H.B., Yoke Wui Ng, M., Thiede, B., Yamamoto, A., Mutugi Nthiga, T., et al. (2019). NIPSNAP1 and NIPSNAP2 act as "eat me" signals for mitophagy. Dev. Cell *49*, 509–525.e12.

97. Schneider, C.A., Rasband, W.S., and Eliceiri, K.W. (2012). NIH Image to ImageJ: 25 years of image analysis. Nat. Methods *9*, 671–675.

STAR★METHODS

KEY RESOURCES TABLE

REAGENT or RESOURCE	SOURCE	IDENTIFIER
Antibodies		
Mouse monoclonal anti-p62-Lck Ligand	BD Biosciences	Cat#610833, RRID: AB_398152
Mouse monoclonal anti-NBR1	Santa Cruz Biotechnology	Cat#sc-130380, RRID: AB_2149402
Rabbit polyclonal anti-TAX1BP1	Sigma-Aldrich	Cat#HPA024432, RRID: AB_1857783
Rabbit polyclonal anti-OPTINEURIN	Sigma-Aldrich	Cat#HPA003360, RRID: AB_1079528
Rabbit polyclonal anti-OPTINEURIN	Abcam	Cat#ab23666, RRID: AB_447598
Rabbit polyclonal anti-MORG1	Sigma-Aldrich	Cat#HPA042838, RRID: AB_10794173
Mouse monoclonal anti-MORG1	Abnova	Cat#H00084292-M02, RRID: AB_1137312
Mouse monoclonal anti-Myc-tag	Cell Signaling Technology	Cat#2276, RRID: AB_331783
Rabbit polyclonal anti-GAPDH	Sigma-Aldrich	Cat#G9545, RRID: AB_796208
Rabbit polyclonal anti-ACTIN	Sigma-Aldrich)	Cat#A2066, RRID: AB_476693
Rabbit polyclonal anti-LC3B	Novus	Cat#NB100-2220, RRID: AB_10003146
Rabbit polyclonal anti-LC3B	Sigma-Aldrich	Cat#L7543, RRID: AB_796155
Rabbit polyclonal anti-GFP	Abcam	Cat#ab290, RRID: AB_303395
Mouse monoclonal anti-HA Tag	Cell Signaling Technology	Cat#3724, RRID: AB_1549585
Mouse monoclonal anti-HIF1A	BD Biosciences	Cat#610959, RRID: AB_398272
Rabbit monoclonal anti-HIF2A	Cell Signaling Technology	Cat#7096, RRID: AB_10898028
Rabbit polyclonal anti-PHD3	Novus	Cat#NB100-139, RRID: AB_2096716
Mouse monoclonal anti-NCOA4	Sigma-Aldrich	Cat#SAB1404569, RRID: AB_10759525
Rabbit monoclonal anti-NDP52	Cell Signaling Technology	Cat#60732, RRID: AB_2732810
Rouse monoclonal anti-GABARAP	MBL International	Cat#M135-3, RRID: AB_10364779
Rabbit monoclonal anti-mTOR	Cell Signaling Technology	Cat#2983, RRID: AB_2105622
Rabbit monoclonal anti-mTOR	Cell Signaling Technology	Cat# 2972, RRID: AB_330978
Rabbit monoclonal anti-Phospho-mTOR (S2448)	Cell Signaling Technology	Cat#2971, RRID: AB_330970
Rabbit polyclonal anti-LAMP1	Sigma-Aldrich	Cat#L1418, RRID: AB_477157
Mouse monoclonal anti-LAMP1	DSHB	Cat#h4a3, RRID: AB_2296838
Mouse monoclonal anti-LAMP2	Santa Cruz Biotechnology	Cat#sc-18822, RRID: AB_626858
Mouse monoclonal anti-LAMP2	DSHB	Cat#h4b4, RRID: AB_528129
Rabbit polyclonal anti-GST	Santa Cruz Biotechnology	Cat#sc-459, RRID: AB_631586
Rabbit monoclonal anti-S6K1	Cell Signaling Technology	Cat#9202, RRID: AB_331676
Rabbit monoclonal anti-Phospho-S6K1	Cell Signaling Technology	Cat#9205, RRID: AB_330944
Rabbit monoclonal anti-4E-BP1	Cell Signaling Technology	Cat#9644, RRID: AB_2097841
Rabbit monoclonal anti-Phospho-4E-BP1	Cell Signaling Technology	Cat#9451, RRID: AB_330947
Rabbit monoclonal anti-ULK1	Cell Signaling Technology	Cat#8054, RRID: AB_11178668
Rabbit monoclonal anti-Phospho-ULK1	Cell Signaling Technology	Cat#6888, RRID: AB_10829226
Rabbit monoclonal anti-AKT	Cell Signaling Technology	Cat#9272, RRID: AB_329827
Rabbit monoclonal anti-Phospho-AKT	Cell Signaling Technology	Cat#9271, RRID: AB_329825
Rabbit monoclonal anti-LAMTOR1	Cell Signaling Technology	Cat#8975, RRID: AB_10860252
Rabbit monoclonal anti-LAMTOR2	Cell Signaling Technology	Cat#8145, RRID: AB_10971636
Rabbit monoclonal anti-LAMTOR3	Cell Signaling Technology	Cat#8168, RRID: AB_10949501
Rabbit monoclonal anti-LAMTOR4	Cell Signaling Technology	Cat#12284, RRID: AB_2797870
Rabbit monoclonal anti-LAMTOR5	Cell Signaling Technology	Cat#14633, RRID: AB_2798547
Rabbit monoclonal anti-RagA	Cell Signaling Technology	Cat#4357, RRID: AB_10545136
Rabbit monoclonal anti-RagB	Cell Signaling Technology	Cat#8150, RRID: AB_11178806
Rabbit monoclonal anti-RagC	Cell Signaling Technology	Cat# 3360, RRID: AB_2180068

(*Continued on next page*)

Continued

REAGENT or RESOURCE	SOURCE	IDENTIFIER
Rabbit monoclonal anti-RagD	Cell Signaling Technology	Cat#4470, RRID: AB_1950380
Rabbit monoclonal anti-TFEB	Cell Signaling Technology	Cat#4240, RRID: AB_11220225
Rabbit monoclonal anti-phospho-TFEB	Cell Signaling Technology	Cat#37681, RRID: AB_2799117
Rabbit monoclonal anti-TFE3 antibody	Cell Signaling Technology	Cat#14779, RRID: AB_2687582
Mouse monoclonal anti-Raptor	Santa Cruz Biotechnology	Cat#sc-81537, RRID: AB_2130791
Rabbit monoclonal anti-GM130	Abcam	Cat#ab52649, RRID: AB_880266
Rabbit polyclonal anti-Calnexin	Abcam	Cat#ab10286, RRID: AB_2069009
Mouse monoclonal IgG1 isotype control	Cell Signaling Technology	Cat#5415, RRID: AB_10829607
Rabbit polyclonal IgG control	Cell Signaling Technology	Cat#2729, RRID: AB_1031062
Rabbit monoclonal IgG isotype control	Cell Signaling Technology	Cat#3900, RRID: AB_1550038
HRP-conjugated anti-GST	Cytiva	Cat#RPN1236, RRID: AB_771429
HRP-conjugated goat anti-rabbit IgG	BD Biosciences	Cat#554021, RRID: AB_395213
HRP-conjugated goat anti-mouse IgG	BD Biosciences	Cat#554002, RRID: AB_395198
Alexa Fluor 555-conjugated goat anti-rabbit IgG	Thermo Fisher Scientific	Cat#A-21428, RRID: AB_2535849
Alexa Fluor 488-conjugated goat anti-rabbit IgG	Thermo Fisher Scientific	Cat#A-11008, RRID: AB_143165
Alexa Fluor 555-conjugated goat anti-mouse IgG	Thermo Fisher Scientific	Cat#A-21424, RRID: AB_141780
Alexa Fluor 488-conjugated goat anti-mouse IgG	Molecular Probes	Cat# A-11029, RRID: AB_2534088
Bacterial and virus strains		
Escherichia coli SoluBL21	Genlantis	Cat#C700200
BL21(DE3)pLysS	Promega,	Cat#L1195
Chemicals, peptides, and recombinant proteins		
Diamidino-2-phenylindole (DAPI)	Thermo Fisher Scientific	62248; CAS: 28718-90-3
DQ-Red BSA	Thermo Fisher Scientific	Cat#D12051
Bafilomycin A1	Sigma-Aldrich	B1793; CAS: 88899-55-2
Z-Leu-Leu-Leu-al (MG132)	Sigma-Aldrich	C2211; CAS: 133407-82-6
Rapamycin	Sigma-Aldrich	R0395; CAS: 53123-88-9
Torin 1	Santa Cruz Biotechnology	sc-396760; CAS: 1222998-36-8
MRT68921 ULK1/2 Inhibitor	Sigma-Aldrich	SML1644; CAS: 1190379-70-4
SAR405 Vps34 Inhibitor	APExBIO	A8883; CAS: 1523406-39-4
HBSS	Sigma-Aldrich	Cat#H8264
Tetracycline	Sigma-Aldrich	87128; CAS: 60-54-8
Doxycycline	Sigma-Aldrich	D9891; CAS: 24390-14-5
Biotin Phenol	Sigma-Aldrich	SML2135; CAS: 41994-02-9
Hydrogen peroxide	Sigma-Aldrich	H1009; CAS: 7722-84-1
Deferiprone	Sigma-Aldrich	379409; CAS: 30652-11-0
Hexadimethrine bromide	Sigma-Aldrich	H9268; CAS: 28728-55-4
CHAPS buffer	Sigma-Aldrich	C3023; CAS: 331717-45-4
Hygromycin	Thermo Fisher Scientific	10687-010; CAS: 31282-04-9
Critical commercial assays		
TNT T7 reticulocyte Lysate system	Promega	Cat#L4610
High-Capacity RNA-to-cDNA Kit	Thermo Fisher Scientific	Cat# 4387406
Pierce BCA Protein Assay Kit	Thermo Fischer Scientific	Cat#23227
RNeasy Mini Kit	Qiagen	Cat#74104
Deposited data		
Raw and analyzed data	This paper/Mendeley data	https://data.mendeley.com/datasets/pwr7wvj4bt/1
Experimental models: Cell lines		
Human: HeLa	ATCC	CCL2

(*Continued on next page*)

Continued

REAGENT or RESOURCE	SOURCE	IDENTIFIER
Human: HEK293	ATCC	CRL-1573
Human: HeLa Flp-In T-REx cells	Sigma-Aldrich	Cat#P4333
Oligonucleotides		
gRNA sequences: MORG1: GTGAGCGGCAATCCCAACAG	This Paper	N/A
gRNA sequences: MORG1: CAGGTCGTGCGCAAATTCCG	This Paper	N/A
gRNA sequences: p62: GGCGCCTCCTGAGCACACGG	This Paper	N/A
gRNA sequences: p62: GTGAGCGACGCCATAGCGAG	This Paper	N/A
qPCR primers: NDP52: TTCTGCTGCCATCCTTGTGG, TCCCAGGGCCCTTGTACTGA	This Paper	N/A
qPCR primers: NBR1: TGCATCCCACAGAAGGCAAA, ACAGCAGGTCCTGGGCAGTC	This Paper	N/A
qPCR primers: TAX1BP1: CGGCCTGATGGCTTAGAGGA, AGCAAAAGCCTGTCCCATGC	This Paper	N/A
qPCR primers: Optineurin: AGGCAGGCAGTCCTTGATGG, CTTGGGGCAGGAATGAATCG	This Paper	N/A
qPCR primers: p62: AAAAGAAGCCGCCTGACCCC, CCTCAACATTCCCACCCGGC	This Paper	N/A
qPCR primers: LC3B: ATAGAACGATACAAGGGTGAG, CTGTAAGCGCCTTCTAATTATC	This Paper	N/A
qPCR primers: Lamin A/C: AGCTGAAAGCGCGCAATACC, GGCCTCCTTGGAGTTCAGCA.	This Paper	N/A
Recombinant DNA		
Gateway pDONR221	Thermo Fisher Scientific	Cat#12536017
Gateway pENTR1A	Thermo Fisher Scientific	Cat#A10462
pENTR223-MORG1	This Paper	N/A
pDestMyc-MORG1	This Paper	N/A
pDest HA-MORG1	This Paper	N/A
pDest MORG1-Myc	This Paper	N/A
pDest MORG1-HA	This Paper	N/A
pDest15 MORG1	This Paper	N/A
pMXs-Puro-MORG1-EGFP	This Paper	N/A
pMRXIP MORG1-EGFP	This Paper	N/A
pMXs-Puro-MORG1-Myc	This Paper	N/A
pMRXIP MORG1-Myc	This Paper	N/A
pMXs-Puro-MORG1-HA	This Paper	N/A
pMRXIP MORG1-HA	This Paper	N/A
pCDH-EF1α-gw-ires-puro-MORG1-EGFP	This Paper	N/A
pCDH-EF1α-gw-ires-puro-MORG1-Myc	This Paper	N/A
pCDH-EF1α-gw-ires-puro-MORG1-HA	This Paper	N/A
PCDNA5/FRT MORG1-EGFP	This Paper	N/A
PCDNA5/FRT MORG1-Myc	This Paper	N/A
PCDNA5/FRT MORG1-HA	This Paper	N/A
pDestMyc-MORG1 1-231	This Paper	N/A
pDestMyc-MORG1 1-190	This Paper	N/A
pDestMyc-MORG1 1-151	This Paper	N/A
pDestMyc-MORG1 23-315	This Paper	N/A
pDestMyc-MORG1 63-315	This Paper	N/A
pDestMyc-MORG1 105-315	This Paper	N/A
pDestMyc-MORG1 147-315	This Paper	N/A

(*Continued on next page*)

Continued

REAGENT or RESOURCE	SOURCE	IDENTIFIER
pCDH-EF1α-gw-ires-puro-MORG1 23-315-Myc	This Paper	N/A
PCW57.1-APEX2	This Paper	N/A
PCW57.1-MORG1-APEX2	This Paper	N/A
pMRXIP LAMP2-mCherry	This Paper	N/A
pMXs-Puro-LAMP2-mCherry	This Paper	N/A
pCDH-EF1α-gw-ires-puro- LAMP2-mCherry	This Paper	N/A
PCDNA5/FRT LAMP2-mCherry	This Paper	N/A
pDestMyc-NBR1	Lamark et al.[91]	N/A
pDestMyc-p62	Lamark et al.[91]	N/A
pDest15 p62	Jain et al.[92]	N/A
pDest15 p62 ΔPB1	Abudu et al.[93]	N/A
pDest15 p62 Δ123-170	Abudu et al.[93]	N/A
pDest15 p62 Δ170-256	Abudu et al.[93]	N/A
pDest15 p62 Δ256-370	Abudu et al.[93]	N/A
pDest15 p62 Δ371-385	Abudu et al.[93]	N/A
pDest15 p62 ΔUBA	Abudu et al.[93]	N/A
pTH1 p62	Clausen et al.[94]	N/A
pCDH-EF1α-gw-ires-puro-Myc-p62	Abudu et al.[93]	N/A
pCDH-EF1α-gw-ires-puro-Myc-p62 Δ170-256	Abudu et al.[93]	N/A
pDest Myc-RagA	This Paper	N/A
pDest Myc-RagB	This Paper	N/A
pDest Myc-RagC	This Paper	N/A
pDest Myc-RagD	This Paper	N/A
pDest HA-RagA	This Paper	N/A
pDest HA-RagB	This Paper	N/A
pDest HA-RagC	This Paper	N/A
pDest HA-RagD	This Paper	N/A
pDest15 RagA	This Paper	N/A
pDest15 RagB	This Paper	N/A
pDest15 RagC	This Paper	N/A
pDest15 RagD	This Paper	N/A
pTH1 RagC	This Paper	N/A
pTH1 RagD	This Paper	N/A
pDest Myc-LAMTOR1	This Paper	N/A
pDest Myc-LAMTOR2	This Paper	N/A
pDest Myc-LAMTOR3	This Paper	N/A
pDest Myc-LAMTOR4	This Paper	N/A
pDest15 LAMTOR1	This Paper	N/A
pDest15 LAMTOR2	This Paper	N/A
pDest15 LAMTOR3	This Paper	N/A
pDest15 LAMTOR4	This Paper	N/A
pDest15 LAMTOR5	This Paper	N/A
pDest15 Galectin 3	This Paper	N/A
pDest15 Galectin 8	This Paper	N/A
pDest15 Galectin 9	This Paper	N/A
pCDH-EF1α-gw-ires-puro-Myc-RagA	This Paper	N/A
pCDH-EF1α-gw-ires-puro-Myc-RagB	This Paper	N/A
pCDH-EF1α-gw-ires-puro-Myc-RagC	This Paper	N/A

(*Continued on next page*)

Continued

REAGENT or RESOURCE	SOURCE	IDENTIFIER
pCDH-EF1α-gw-ires-puro-Myc-RagD	This Paper	N/A
pCDH-EF1α-gw-ires-puro-Myc-RagA T21L	This Paper	N/A
pCDH-EF1α-gw-ires-puro-Myc-RagA Q66L	This Paper	N/A
pCDH-EF1α-gw-ires-puro-Myc-RagB T54L	This Paper	N/A
pCDH-EF1α-gw-ires-puro-Myc-RagB Q99L	This Paper	N/A
pCDH-EF1α-gw-ires-puro-Myc-RagC S75L	This Paper	N/A
pCDH-EF1α-gw-ires-puro-Myc-RagC Q120L	This Paper	N/A
pCDH-EF1α-gw-ires-puro-Myc-RagD S77L	This Paper	N/A
pCDH-EF1α-gw-ires-puro-Myc-RagD Q121L	This Paper	N/A
Software and algorithms		
ImageJ	Schneider et al.[95]	https://imagej.nih.gov/ij/
Prism 10	GraphPad Software	https://www.graphpad.com/
Canvas X	Canvas GFX	https://www.canvasgfx.com/products/canvas-x-draw
ScienceLab ImageGuage	FujiFilm	N/A
Other		
cOmplete Mini EDTA-free protease inhibitor cocktail tablets	Roche Applied Science	Cat#11836170001
Myc-TRAP	Chromotek	Cat# yta-20
Glutathione Sepharose 4 Fast Flow beads	GE Healthcare	Cat#17-5132-01
Amylose Resin	New England Biolabs	Cat#E8021L
Coomassie Brilliant Blue R-250 Dye	Thermo Fisher Scientific	Cat#20278

RESOURCE AVAILABILITY

Lead contact

Further information and requests for resources and reagents should be directed to and will be fulfilled by the lead contact Terje Johansen (terje.johansen@uit.no).

Materials availability

All plasmids and cell lines generated in this study are available upon request from the lead contact.

Data and code availability

All original source files (microscopy images and blots) have been deposited in Mendeley data and available on https://data.mendeley.com/datasets/pwr7wvj4bt/1. All data are publicly available as of the date of publication. Accession numbers and DOI are listed in the key resources table.

This paper does not report any original code.

Any additional information required to reanalyze the data reported in this paper is available from the lead contact upon request.

EXPERIMENTAL MODEL AND STUDY PARTICIPANT DETAILS

Cell line models

Human cells (HeLa and HEK293) were obtained from ATCC. p62 KO MEFs were a kind gift from Masaaki Komatsu. All cells were maintained in DMEM supplemented with 10% fetal bovine serum and 1% penicillin/Streptomycin.

METHOD DETAILS

Antibodies and reagents

The following primary antibodies were used: mouse monoclonal anti-p62-Lck Ligand antibody (BD Bioscience, #610833), mouse monoclonal anti-NBR1 antibody (Santa Cruz, #sc-130380), rabbit polyclonal anti-TAX1BP1 antibody (Sigma, #HPA024432), rabbit polyclonal anti-OPTINEURIN antibody (Sigma, #HPA003360), rabbit polyclonal anti-OPTINEURIN antibody (Abcam, #ab23666), rabbit polyclonal anti-MORG1 antibody (Sigma, #HPA042838), mouse monoclonal anti-MORG1 antibody (Abnova, #H00084292-M02), mouse monoclonal anti-Myc-tag antibody (Cell signal., #2276), rabbit polyclonal anti-GAPDH antibody (Sigma, #G9545), rabbit

polyclonal anti-ACTIN antibody (Sigma, #A2066), rabbit polyclonal anti-LC3B antibody (Novus Bio., #NB100-2220), rabbit polyclonal anti-LC3B antibody (Sigma, #L7543), rabbit polyclonal anti-GFP antibody (Abcam, #ab290), mouse monoclonal anti-FLAG M2 antibody (Sigma, #F1804), mouse monoclonal anti-HA Tag antibody (Roche, #11583816001), rabbit monoclonal anti-HA Tag antibody (Cell Signal, #3724S), mouse monoclonal anti-HIF1A antibody (BD Bioscience, #610959), rabbit monoclonal anti-HIF2A antibody (Cell Signal, #7096), rabbit polyclonal anti-PHD3 antibody (Novus Bio., # NB100-139), mouse monoclonal anti-NCOA4 antibody (Sigma, #SAB-1404569), rabbit monoclonal anti-NDP52 antibody (Cell Signal., #60732), mouse monoclonal anti-GABARAP antibody (MBL, #M135-3), rabbit monoclonal anti-mTOR antibody (Cell Signal, #2983), rabbit monoclonal anti-mTOR antibody (Cell Signal, #2972), rabbit monoclonal anti-Phospho-mTOR antibody (Cell Signal, #2971), rabbit polyclonal anti-LAMP1 antibody (Sigma, #L1418), mouse monoclonal anti-LAMP1 antibody (DSHB, #H4A3), mouse monoclonal anti-LAMP2 antibody (Santa Cruz, #sc-18822), mouse monoclonal anti-LAMP2 antibody (DSHB, #H4B4), rabbit polyclonal anti-GST antibody (Santa Cruz, #sc-459), rabbit monoclonal anti-S6K1 antibody (Cell Signal, #9202), rabbit monoclonal anti-Phospho-S6K1 antibody (Cell Signal, #9205), rabbit monoclonal anti-4E-BP1 antibody (Cell Signal, #9644), rabbit monoclonal anti-Phospho-4E-BP1 antibody (Cell Signal, #9451), rabbit monoclonal anti-ULK1 antibody (Cell Signal, #8054), rabbit monoclonal anti-Phospho-ULK1 antibody (Cell Signal, #6888), rabbit monoclonal anti-AKT antibody (Cell Signal, #9272), rabbit monoclonal anti-Phospho-AKT antibody (Cell Signal, #9271), rabbit monoclonal anti-LAMTOR1 antibody (Cell Signal, #8975), rabbit monoclonal anti-LAMTOR2 antibody (Cell Signal, #8145), rabbit monoclonal anti-LAMTOR3 antibody (Cell Signal, #8168), rabbit monoclonal anti-LAMTOR4 antibody (Cell Signal, #12284), rabbit monoclonal anti-LAMTOR5 antibody (Cell Signal, #14633), rabbit monoclonal anti-RagA antibody (Cell Signal, #4357), rabbit monoclonal anti-RagB antibody (Cell Signal, #8150), rabbit monoclonal anti-RagC antibody (Cell Signal, #3360), rabbit monoclonal anti-RagD antibody (Cell Signal, #4470), rabbit monoclonal anti-TFEB antibody (Cell Signal, #4240), rabbit monoclonal anti-p-TFEB antibody (Cell Signal, #37681), rabbit monoclonal anti-TFE3 antibody (Cell Signal, #14779), mouse monoclonal anti-Raptor antibody (Santa Cruz, #sc-81537), rabbit monoclonal anti-GM130 antibody (Abcam, #ab52649), rabbit polyclonal anti-Calnexin antibody (Abcam, #ab10286), mouse monoclonal IgG1 isotype control antibody (Cell Signal, #5415), rabbit polyclonal IgG control antibody (Cell Signal, #2729), rabbit monoclonal IgG isotype control antibody (Cell Signal, #3900). Secondary antibodies include HRP-conjugated anti-GST antibody (Sigma, #GERPN1236), HRP-conjugated goat anti-rabbit IgG (BD Bioscience, #554021), HRP-conjugated goat anti-mouse IgG (BD Bioscience, #554002), Alexa Fluor 555-conjugated goat anti-rabbit IgG (Thermo Fisher Scientific, #A-21428), Alexa Fluor 488-conjugated goat anti-rabbit IgG (Thermo Fisher Scientific, #A-11008), Alexa Fluor 555-conjugated goat anti-mouse IgG (Thermo Fisher Scientific, #A-21424), Alexa Fluor 488-conjugated goat anti-mouse IgG (Thermo Fisher Scientific, #A-11029). Reagents: Diamidino-2-phenylindole (DAPI) (Thermo Fisher Scientific, #62248), DQ-Red BSA (Invitrogen, #D12051), Bafilomycin A1 (Sigma, #B1793), MG132 (Z-Leu-Leu-Leu-al) (Sigma, #C2211), Rapamycin (Sigma, #R0395), Torin 1 (Santa Cruz, #sc-396760), MRT68921 (Sigma, #SML1644), SAR405 (APExBIO, #A8883), Hanks Balanced salt solution (Sigma, #H8264), Hygromycin (Thermo Fisher Scientific, #10687-010), Tetracycline, (Sigma, #87128), Doxycycline (Sigma, #D9891), Biotin Phenol (Sigma, #SML2135), Hydrogen peroxide (Sigma, #H1009) and Deferiprone (Sigma, #379409)

Plasmids

Plasmids used in this study are presented in the table below. Details are available on request. Gateway BP and LR recombination reactions were done according to instruction in the gateway-cloning manual (Thermo Fisher Scientific). Point mutations and deletions were carried out by site directed mutagenesis. PCR and sequencing oligonucleotides were designed and ordered from Sigma. Restriction digestion and DNA sequencing (BigDye, Applied Biosystems, #4337455) were used to verify all plasmids.

Vector	Description	Source
pDONR221	Gateway donor vector	Thermo Fisher
pENTR1A	Gateway entry vector	Thermo Fisher
pDestMyc	Mammalian N-terminal Myc-tag fusion expression vector with CMV and T7 promoters	Lamark et al.[91]
PDestMyc-N1	Mammalian C-terminal Myc-tag fusion expression vector with CMV and T7 promoters	Lamark et al.[91]
pDest15	Bacterial GST-fusion expression vector with a T7 promoter	Thermo Fisher
pENTR223-MORG1	Human MORG1 in Gateway entry vector.	This study
pDestMyc-MORG1	Human MORG1 with N-terminal Myc tag	This study
pDest HA-MORG1	Human MORG1 with N-terminal HA tag	This study
pDest MORG1-Myc	Human MORG1 with C-terminal Myc tag	This study
pDest MORG1-HA	Human MORG1 with C-terminal HA tag	This study
pDest15 MORG1	Human MORG1 with N-terminal GST fusion tag	This study
pMXs-Puro-MORG1-EGFP	Retroviral vector with Human MORG1 and C-terminal EGFP tag	This study

(*Continued on next page*)

Continued

Vector	Description	Source
pMRXIP MORG1-EGFP	Retroviral vector with Human MORG1 and C-terminal EGFP tag	This study
pMXs-Puro-MORG1-Myc	Retroviral vector with Human MORG1 and C-terminal Myc tag	This study
pMRXIP MORG1-Myc	Retroviral vector with Human MORG1 and C-terminal Myc tag	This study
pMXs-Puro-MORG1-HA	Retroviral vector with Human MORG1 and C-terminal HA tag	This study
pMRXIP MORG1-HA	Retroviral vector with Human MORG1 and C-terminal MHA tag	This study
pCDH-EF1α-gw-ires-puro-MORG1-EGFP	Lentiviral vector with MORG1 and C-terminal EGFP tag	This study
pCDH-EF1α-gw-ires-puro-MORG1-Myc	Lentiviral vector with MORG1 and C-terminal Myc tag	This study
pCDH-EF1α-gw-ires-puro-MORG1-HA	Lentiviral vector with MORG1 and C-terminal HA tag	This study
PCDNA5/FRT MORG1-EGFP	Flip-In vector with Human MORG1 and C-terminal EGFP tag	This study
PCDNA5/FRT MORG1-Myc	Flip-In vector with Human MORG1 and C-terminal Myc tag	This study
PCDNA5/FRT MORG1-HA	Flip-In vector with Human MORG1 and C-terminal HA tag	This study
pDestMyc-MORG1 1-231	Human MORG1 amino acid 1-231 with N-terminal Myc tag	This study
pDestMyc-MORG1 1-190	Human MORG1 amino acid 1-190 with N-terminal Myc tag	This study
pDestMyc-MORG1 1-151	Human MORG1 amino acid 1-151 with N-terminal Myc tag	This study
pDestMyc-MORG1 23-315	Human MORG1 amino acid 23-315 with N-terminal Myc tag	This study
pDestMyc-MORG1 63-315	Human MORG1 amino acid 63-315 with N-terminal Myc tag	This study
pDestMyc-MORG1 105-315	Human MORG1 amino acid 105-315 with N-terminal Myc tag	This study
pDestMyc-MORG1 147-315	Human MORG1 amino acid 147-315 with N-terminal Myc tag	This study
pCDH-EF1α-gw-ires-puro-MORG1 23-315-Myc	Lentiviral vector with MORG1 amino acid 23-315 and C-terminal Myc tag	This study
PCW57.1-APEX2	Lentiviral vector with an engineered ascorbate peroxidase	This Study
PCW57.1-MORG1-APEX2	Lentiviral vector with Human MORG1 tagged C-terminally with an engineered ascorbate peroxidase	This Study
pMRXIP LAMP2-mCherry	Retroviral vector with Human LAMP2 and C-terminal mCherry tag	This study
pMXs-Puro-LAMP2-mCherry	Retroviral vector with Human LAMP2 and C-terminal mCherry tag	This study
pCDH-EF1α-gw-ires-puro- LAMP2-mCherry	Lentiviral vector with LAMP2 and C-terminal mCherry tag	This study
PCDNA5/FRT LAMP2-mCherry	Flip-In vector with Human LAMP2 and C-terminal mCherry tag	This study
pDestMyc-NBR1	Human NBR1 with N-terminal Myc tag	Lamark et al.[91]
pDestMyc-p62	Human p62 with N-terminal Myc tag	Lamark et al.[91]
pDest15 p62	Human p62 with N-terminal GST fusion tag	Jain et al.[92]
pMXs-Neo-3xFLAG p62	Retroviral vector with Human p62 and N-terminal 3xFLAG tag	Abudu et al.[93]
pDest15 p62 ΔPB1	Human p62 with PB1 domain deletion and N-terminal GST fusion tag	Abudu et al.[93]
pDest15 p62 Δ123-170	Human p62 with 123-170 deletion and N-terminal GST fusion tag	Abudu et al.[93]
pDest15 p62 Δ170-256	Human p62 with 170-256 deletion and N-terminal GST fusion tag	Abudu et al.[93]
pDest15 p62 Δ256-370	Human p62 with 256-370 deletion and N-terminal GST fusion tag	Abudu et al.[93]
pDest15 p62 Δ371-385	Human p62 with 371-385 deletion and N-terminal GST fusion tag	Abudu et al.[93]
pDest15 p62 ΔUBA	Human p62 with UBA domain deletion and N-terminal GST fusion tag	Abudu et al.[93]
pTH1 p62	Human p62 with N-terminal MBP fusion tag	Abudu et al.[94]
pCDH-EF1α-gw-ires-puro-Myc-p62	Lentiviral vector with p62 and N-terminal Myc tag	Abudu et al.[93]
pCDH-EF1α-gw-ires-puro-Myc-p62 Δ170-256	Lentiviral vector with p62 Δ170-256 and N-terminal mCherry tag	Abudu et al.[93]
pDest Myc-RagA	Human RagA with N-terminal Myc tag	This study
pDest Myc-RagB	Human RagB with N-terminal Myc tag	This study
pDest Myc-RagC	Human RagC with N-terminal Myc tag	This study
pDest Myc-RagD	Human RagD with N-terminal Myc tag	This study
pDest HA-RagA	Human RagA with N-terminal HA tag	This study
pDest HA-RagB	Human RagB with N-terminal HA tag	This study
pDest HA-RagC	Human RagC with N-terminal HA tag	This study
pDest HA-RagD	Human RagD with N-terminal HA tag	This study
pDest15 RagA	Human RagA with N-terminal GST fusion tag	This study

(*Continued on next page*)

Continued

Vector	Description	Source
pDest15 RagB	Human RagB with N-terminal GST fusion tag	This study
pDest15 RagC	Human RagC with N-terminal GST fusion tag	This study
pDest15 RagD	Human RagD with N-terminal GST fusion tag	This study
pTH1 RagC	Human RagC with N-terminal MBP fusion tag	This study
pTH1 RagD	Human RagD with N-terminal MBP fusion tag	This study
pDest Myc-LAMTOR1	Human LAMTOR1 with N-terminal Myc tag	This study
pDest Myc-LAMTOR2	Human LAMTOR2 with N-terminal Myc tag	This study
pDest Myc-LAMTOR3	Human LAMTOR3 with N-terminal Myc tag	This study
pDest Myc-LAMTOR4	Human LAMTOR4 with N-terminal Myc tag	This study
pDest15 LAMTOR1	Human LAMTOR1 with N-terminal GST fusion tag	This study
pDest15 LAMTOR2	Human LAMTOR2 with N-terminal GST fusion tag	This study
pDest15 LAMTOR3	Human LAMTOR3 with N-terminal GST fusion tag	This study
pDest15 LAMTOR4	Human LAMTOR4 with N-terminal GST fusion tag	This study
pDest15 LAMTOR5	Human LAMTOR4 with N-terminal GST fusion tag	This study
pDest15 Galectin 3	Human Galectin 3 with N-terminal GST fusion tag	This study
pDest15 Galectin 8	Human Galectin 8 with N-terminal GST fusion tag	This study
pDest15 Galectin 9	Human Galectin 9 with N-terminal GST fusion tag	This study
pCDH-EF1α-gw-ires-puro-Myc-RagA	Lentiviral vector with RagA and N-terminal Myc tag	This study
pCDH-EF1α-gw-ires-puro-Myc-RagB	Lentiviral vector with RagB and N-terminal Myc tag	This study
pCDH-EF1α-gw-ires-puro-Myc-RagC	Lentiviral vector with RagC and N-terminal Myc tag	This study
pCDH-EF1α-gw-ires-puro-Myc-RagD	Lentiviral vector with RagD and N-terminal Myc tag	This study
pCDH-EF1α-gw-ires-puro-Myc-RagA T21L	Lentiviral vector with RagA T21L and N-terminal Myc tag	This study
pCDH-EF1α-gw-ires-puro-Myc-RagA Q66L	Lentiviral vector with RagA Q66L and N-terminal Myc tag	This study
pCDH-EF1α-gw-ires-puro-Myc-RagB T54L	Lentiviral vector with RagB T54L and N-terminal Myc tag	This study
pCDH-EF1α-gw-ires-puro-Myc-RagB Q99L	Lentiviral vector with RagB Q99L and N-terminal Myc tag	This study
pCDH-EF1α-gw-ires-puro-Myc-RagC S75L	Lentiviral vector with RagC S75L and N-terminal Myc tag	This study
pCDH-EF1α-gw-ires-puro-Myc-RagC Q120L	Lentiviral vector with RagC Q120L and N-terminal Myc tag	This study
pCDH-EF1α-gw-ires-puro-Myc-RagD S77L	Lentiviral vector with RagD S77L and N-terminal Myc tag	This study
pCDH-EF1α-gw-ires-puro-Myc-RagD Q121L	Lentiviral vector with RagD Q121L and N-terminal Myc tag	This study

Cell culture and treatments

HeLa (ATCC, CCL2) and HeLa Flp-In T-REx cells (Thermo Fisher Scientific, R714-07) were grown in DMEM (Sigma, #D5796) supplemented with 10% FBS (Biochrom AG, #S0615) and 1% streptomycin-penicillin (Sigma, #P4333). HEK293 (ATCC, CRL-1573) and MEF cells were grown in DMEM (Sigma, #D6046) supplemented with 10% FBS and 1% streptomycin-penicillin. Cells were tested regularly for Mycoplasma. Cells were treated with 0.2μM Bafilomycin A1 (BafA1) and 1mM DFP for indicated durations.

Generation of human KO cell lines using CRISPR/Cas9 System

CRISPR/cas9-mediated knockout and knockdown were generated as described.[93] Small guide RNA (sgRNA) targeting different exons of indicated proteins were annealed and ligated into Bbs1 linearized vectors carrying a wild-type CRISPR-associated protein 9 (Cas9) and either green fluorescent protein (GFP) (Addgene, #48138) or puromycin resistance gene (Addgene, #62988). HeLa and HEK293 cells were seeded into 6cm plates and transfected with the sgRNA-containing Cas9 vector using Metafectene Pro (Biontex #T040). 24h after transfection, cells were selected by treatment with 1-2mg/ml puromycin for 36hrs for vectors carrying the puromycin gene or sorted using GFP signal. Single clones were sorted into 96-well plates and expanded. Knockdown and/or knockout were screened by immunoblotting and/or genomic analysis. For genomic analysis, DNA were extracted using the Genelute mammalian genomic DNA miniprep kit (Sigma #G1N350) and the area of interest amplified by polymerase chain reaction (PCR). The PCR-amplified region of interest was ligated into the pGEM-T vector (Promega #A3600) and sequenced to identify insertions or deletions (indels). CRISPR gRNA primers used include; MORG1, GTGAGCGGCAATCCCAACAG, CAGGTCGTGCGCAAATTCCG; p62, GGCGC CTCCTGAGCACACGG, GTGAGCGACGCCATAGCGAG.

Generation of stable cell lines and reconstitution of KO cell lines

Stable and reconstituted cell lines were generated using either the FlpIn TREx system (Thermo Fisher Scientific, #R71407) or viral transduction. For FlpIn TREx cell lines, cDNAs were first PCR-amplified and then ligated into the inducible FlpIn expression vector, pCDNA5/FRT/TO. FlpIn TREx cells were co-transfected with the FlpIn expression vector containing the cDNA and the Flp recombinase vector pOG44 in a ratio of 1:3. Transfected cells were selected by treatment with 200 μg/ml hygromycin, and protein expression verified by induction with tetracycline or doxycycline. For retroviral transduction, pMXs vectors (Cell Biolabs, #RTV-011 and RTV-012) and pMRXIP (Backbone; Addgene, #45909) were used. For lentiviral transduction, pCDH-EF1alpha-GW-IRES-PURO or pCDH-EF1alpha-GW-IRES-NEO vector were used.[95] cDNAs were either amplified by PCR and ligated into the viral vectors or inserted by GATEWAY recombination. These vectors were transfected into either the HEK293 Phoenix cells for retroviral packaging or HEK293T, together with the packaging vectors pMD2.G and psPAX2 for Lentiviral packaging. The resulting viral particles were mixed with 8 μg/ml hexadimethrine bromide (Sigma, #H9268) and used to transduce cells. Cells were selected and maintained in appropriate antibiotics to optimize protein expression.

Immunoblotting, immunoprecipitation, and mass spectrometry

For immunoblotting, cells were seeded in either 6cm or 10cm dish and treated as indicated. Cells were lysed in 2xSDS buffer (50 mM Tris pH 7.4, 2% SDS, 10% Glycerol) supplemented with 200 mM dithiothreitol (DTT, Sigma, #D0632) and heated at 100°C for 10 min. Protein concentration was measured using the Pierce BCA Protein Assay Kit (Thermo Fischer Scientific, #23227).10-60 μg of protein was resolved by SDS-PAGE and transferred to nitrocellulose membrane (Sigma, # GE10600003). The membrane was first blocked with 5% non-fat dry milk or bovine serum albumin (BSA, Sigma, #A7906) in 1% TBS-T (0.2M Tris (pH8.0), 1.5 M NaCl and 0.05% Tween-20 (Sigma, #P9416)) and then incubated with indicated primary antibodies for 24h. The membrane was washed three times for 10 min each with TBS-T followed by incubation with secondary antibody for 1h. The membrane was washed three times for 10 min and analyzed by enhanced chemiluminescence using the ImageQuant LAS 4000 (GE Healthcare). For immunoprecipitation, cells were lysed in either modified radioimmunoprecipitation assay (RIPA) buffer (50 mM Tris-Cl, pH 7.4, 120 mM NaCl, 1 mM EDTA pH 8.0, 1% NP-40, 0.25% Triton X-100) or in CHAPS buffer (0.3% CHAPS (Sigma, #C3023), 40mM HEPES (pH 7.4), 2.5mM $MgCl_2$) supplemented with cOmplete Mini EDTA-free protease inhibitor cocktail tablets (Roche Applied Science, #11836170001) and phosphatase inhibitor cocktail (Merck Millipore, #524625) by shaking at 4°C for 30 min. The cell lysate was then centrifuged at 10.000 x g for 10 min. The resulting supernatant was incubated with Myc-TRAP (Chromotek, #yta-20) or GFP-TRAP (Chromotek, #gta-20) for cells stably expressing Myc-tagged or GFP-tagged proteins respectively or with anti-FLAG M2 affinity gel (Sigma, #A2220) for cells stably expressing 3xFLAG-tagged proteins. This was followed by either immunoblotting or protein identification by Mass spectrometry. Protein identification by liquid-chromatography-mass spectrometry (LC-MS/MS) was performed as described earlier.[96]

APEX2 proximity labelling and Streptavidin enrichment for mass spectrometry

HeLa cells stably expressing either APEX2 or MORG1-APEX2 were incubated with 500uM biotin-phenol (AdipoGen) for 30 minutes followed by a quick 1-minute pulse with 1mM hydrogen peroxide (H_2O_2) at room temperature. Reaction was stopped with quenching buffer buffer (10mM sodium ascorbate, 10mM sodium azide and 5mM Trolox in PBS). The samples were then washed twice with quenching buffer and twice with PBS. For mass spectrometric analysis (LC-MS/MS), cells were lysed in 500 μl ice-cold lysis buffer (6M urea, 0.3M NaCl, 1mM EDTA, 1mM EGTA, 10mM sodium ascorbate, 10mM sodium azide, 5mM Trolox, 1% glycerol and 25mM Tris-HCl, pH7.5) for 30min by gentle pipetting. The lysates were then clarified by centrifugation and protein concentration determined using Pierce protein assay. Streptavidin-coated magnetic beads (Pierce, #88816) were first washed with lysis buffer and 3mg of each sample were mixed with 100 μl of streptavidin beads and rotated gently overnight at 4^0C to bind biotinylated proteins. After enrichment, the suspension was then passed through a magnetic stand and the flow through removed. The beads were then washed in sequence; twice in 1ml IP buffer (150mM NaCl, 10mM Tris-HCl, pH8.0, 1mM EDTA, 1mM EGTA, 1% Triton X-100), once with 1ml 1M KCl; once with 1ml of 50mM Na_2CO_3; once with 1ml 2M urea in 20mM Tris HCl, pH8.0; and then once with 1ml IP buffer again. The protein samples on beads were further washed four times with 200ul of 50mM Triethyl ammonium bicarbonate (TEAB) for 20 minutes at 4^0C. The samples were first predigested with 1ug of trypsin in 150ul of 50mM TEAB and 1mM $CaCl_2$ on a shaker at 800rpm for 1hour at room temperature. 5mM DTT (dithiothreitol) was added and further shaked for 45 minutes at room temperature. 15mM iodoacetamide was added and the mixture was incubated in the dark on a shaker for 30 minutes followed by 5mM DTT. 2ug of trypsin was then added to the mixture and incubated on a shaker at 800rpm at 37^0C overnight before they are processed for LC-MS (See Protein identification by liquid-chromatography-mass spectrometry Mass (LC-MS/MS) described earlier)

Confocal microscopy

Cells were seeded on coverslips (VWR, #631-0150) in 24-well plates and treated as indicated. Cells were then fixed in 4% paraformaldehyde for 10 min and permeabilized in 0.1% TritonX-100 for 5 min at room temperature. Cells were blocked in 3% goat serum for 30 min before incubation in primary antibodies for 1h at room temperature, followed by washing five times with PBS for five min each. The cells were then incubated with the corresponding Alexa Fluor-conjugated secondary antibodies for 30 min at room temperature followed by washing with PBS for five times. Finally, the cells were incubated with 10 μg/ml of DAPI for 10 min. Slides were mounted with VectaShield antifade mounting media (Vector, #H-1000). For live cell imaging, cells were grown in 8-well Lab-Tek II Chambered

Cover glasses (Thermo Fisher Scientific, #155360) and treated as indicated. Images were obtained using a 40x/NA1.2 water immersion objective, or a 63x/NA1.4 oil immersion objective on an LSM800 system (Carl Zeiss Microscopy). For quantitative analysis, 50-100 cells were randomly selected per sample and quantified as indicated using the ImageJ software.

Recombinant protein expression, in vitro translation and GST-pull-down assay

GST- and MBP-fusion proteins were expressed in competent *Escherichia coli* SoluBL21 (Genlantis, #C700200) and BL21(DE3)pLysS (Promega, #L1195). Protein expression was induced by treating overnight bacterial culture with 50 μg/ml Isopropyl β-D-1-thiogalactopyranoside (IPTG), and expressed protein purified by immobilization on either Glutathione Sepharose 4 Fast Flow beads (GE Healthcare, #17-5132-01) for GST-fusion protein or Amylose Resin (New England Biolabs, #E8021L) for MBP fusion protein. For pull-down assay, Myc-tagged proteins were translated *in vitro* using the TNT T7 reticulocyte Lysate system (Promega, #L4610) in the presence of radioactive ^{35}S-methionine. 10 μl of the translated protein were first precleared with either empty gluthathione sepharose or amylose beads in NETN buffer (50 mM Tris pH 8.0, 150 mM NaCl, 1 mM EDTA, 0.5% NP-40) supplemented with cOmplete Mini EDTA-free protease inhibitor cocktail tablets at 4°C for 30 min to remove unspecific binding. This was followed by incubation with the GST or MBP-fusion proteins at 4°C for 1-2h. The beads were washed five times with 500 μl NETN buffer by centrifugation at 2500 x g for 2 min. 2xSDS gel loading buffer (100 mM Tris pH 7.4, 4% SDS, 20% glycerol, 0.2% Bromophenol blue and 200 mM dithiothreitol DTT (Sigma, #D0632) was added and the mixture heated for 10 min at 100°C. The assay was resolved by SDS-PAGE and the gel stained with Coomassie Brilliant Blue R-250 Dye (Thermo Fisher Scientific, #20278) to visualize the fusion proteins. The stained gel was vacuum dried, and the radioactive signal detected by a Fujifilm bioimaging analyzer BAS-5000 (Fujifilm).

Lysosomal immunoprecipitation assay

Lysosomal Immunoprecipitation assay was performed as earlier described.[85] HeLa WT and MORG1 KO cells stably expressing TMEM192-3×HA or TMEM192-2×FLAG were grown in 15cm dish and used for the assay. Cells were rinsed twice with PBS and scraped in 1ml of KPBS buffer (136mM KCl, 10mM KH2PO4, pH7.25, adjusted with KOH) followed by centrifugation at 1000xg for 2 minutes at 4°C. Cell pellets were resuspended in 1mk KPBS buffer and gently homogenized in a 2ml glass homogenizer with 20 strokes. The cell homogenates were then centrifuged at 1000xg for 2 minutes at 4°C and 50ul of sample was saved as input. The rest of the sample were incubated with 150μl of anti-HA affinity Matrix (Roche, #11815016001) and rotated for 10 minutes. The immunoprecipitates were washed three times with KPBS buffer, eluted in 2x SDS buffer and analyzed by immunoblotting.

Serum and amino acid stimulation of cells

HeLa and HEK293 cells were cultured in 6cm or 10cm plates and rinsed with twice PBS. For serum stimulation, cells were first incubated in serum free RPMI 1640 media (Sigma, #8758) for 60 minutes followed by stimulation with RPMI media with 10% serum for 10 or 20 minutes. For leucine and amino acid stimulation of WT and MORG1 KO cells, cells were incubated in serum and amino acid (or leucine)-free RPMI 1640 (USBio, #R8999-04A and Sigma, #R1780) for 60 minutes, followed by stimulation with different concentration of amino acid or leucine as indicated. For leucine or amino acid stimulation of HeLa WT and p62 KO cells, cells were incubated in serum and amino acid-free RPMI 1640 for 4 hours, followed by stimulation with leucine or amino acid for indicated time. Cell lysates were then analyzed by immunoprecipitation and/or immunoblotting.

Incucyte-based cell proliferation and migration assay

For cell proliferation assays, Cells grown in a 96 well Incucyte ImageLock plates (Sartorius, #4806) were analyzed in the Incucyte live cell imager. Images were acquired every 2 hours for the duration of the experiment. For the migration assay, cells seeded in 96-well Incucyte ImageLock plates were grown to about 90% confluency and scratched using the Incucyte wound marker tool and images acquired every 2 hours for the duration of the experiment. Breast cancer cells transfected with either control gRNA or MORG1 gRNA containing vector carrying the wild type CRISPR-associated protein 9 (Cas9) and puromycin resistance genes (Addgene, #62988) were selected with 1μg/ml of puromycin until all the non-transfected control cells were dead. Colonies of surviving cells were expanded and subjected to proliferation and scratch assay as described above. Images were then analyzed using the Incucyte base analysis software and Incucyte plate map editor.

Dye quenched-Bovine serum albumin trafficking assay

HeLa cells were seeded on coverslips (VWR, #631-0150) in 24-well plates and grown to 70% confluency. Cells were incubated for six (6) hours with 10μg/ml of DQ-Red BSA (Thermo Fisher Scientific, #D12051) in DMEM (Sigma, #D6046) supplemented with 10% FBS and 1% streptomycin-penicillin to allow for effective trafficking. Cells were then fixed with 4% paraformaldehyde for 10 min and nucleus stained with DAPI. Images were obtained with a 63x/NA1.4 oil immersion objective on an LSM800 system (Carl Zeiss Microscopy). For quantitative analysis, 50-100 cells were randomly selected per sample and quantified as indicated using the ImageJ software.

RT-qPCR analysis

mRNA was extracted from cells using RNeasy Mini Kit (Qiagen), with a DNase I (Qiagen) digestion step to minimize genomic DNA contamination. Reverse transcription (RT) was done using High-Capacity RNA-to-cDNA Kit (Thermo-Fisher), and then quantitative

PCR (qPCR) was performed using the BioRad T100 Thermal Cycler System. Results were normalized to Lamin A/C. The following primers (Forward and Reverse) were used: NDP52: TTCTGCTGCCATCCTTGTGG, TCCCAGGGCCCTTGTACTGA, NBR1: TGCATC CCACAGAAGGCAAA, ACAGCAGGTCCTGGGCAGTC, TAX1BP1 CGGCCTGATGGCTTAGAGGA, AGCAAAAGCCTGTCCCATGC, OPTN: AGGCAGGCAGTCCTTGATGG, CTTGGGGCAGGAATGAATCG, LC3B: ATAGAACGATACAAGGGTGAG, CTGTAAGCGCC TTCTAATTATC, p62: AAAAGAAGCCGCCTGACCCC, CCTCAACATTCCCACCCGGC, Lamin A/C: AGCTGAAAGCGCGCAATACC, GGCCTCCTTGGAGTTCAGCA.

QUANTIFICATION AND STATISTICAL ANALYSIS

Descriptive and analytical statistics were generated in Prism 9 software (GraphPad). Quantitative analyses were performed by ScienceLab ImageGuage software (Fujifilm) and Image J (US National Institutes of Health).[97] All data are presented as mean ± SD. Statistical comparison was analyzed by either analysis of variance (ANOVA) with Turkey's HSD post hoc test or a two tailed student t test. Statistical significance displayed as ***$p < 0.001$, **$p < 0.005$, *$p < 0.01$; NS is not significant.